

Large-scale exponential correlations of non-affine elastic response of strongly disordered materials

D. A. Conyuh, D. V. Babin, I. O. Raikov, and Y. M. Beltukov*
Ioffe Institute, Politechnicheskaya st. 26, 194021 St. Petersburg, Russia
 (Dated: May 8, 2025)

The correlation properties of non-affine elastic response in strongly disordered materials are investigated using the theory of correlated random matrices and molecular dynamics simulations. The random matrix theory shows that the divergence of the non-affine displacement field has large-scale exponentially decaying correlations. The corresponding length scale ξ is determined by the strength of the disorder and can be indefinitely large, significantly exceeding the correlation length of the disorder. The rotor of the non-affine displacement field has the same length scale ξ except the case of the volumetric deformation. The main theoretical dependencies are confirmed by molecular dynamics simulation of a model polystyrene in the amorphous state.

I. INTRODUCTION

Interest in studying the nature of the amorphous solid state and its microscopic structure has not waned over the decades [1–3]. The properties of vibrational excitations and the local elastic properties of amorphous materials are the subject of active research [4, 5]. The random atomic arrangement in amorphous (glassy) materials significantly influences their behavior on both the nanoscale and macroscopic levels, with microscopic elastic properties displaying noticeable spatial inhomogeneity and diverging considerably from those found in crystalline materials [6–9]. Such properties encompass the phenomenon of *non-affine* atomic displacements.

In a perfectly ordered structure, such as Bravais lattices, a uniform macroscopic deformation leads to an affine displacement, with the displacement of each atom proportional to its position. In this case, the forces acting on a single atom from its nearest neighbors can cancel each other out due to symmetry, and there are no resulting local forces, only macroscopic ones [10]. In contrast, in a disordered structure, there are non-zero local forces acting on each atom, causing additional local displacements called non-affine [10–12]. The presence of non-affine displacements was observed in a wide range of amorphous materials: metallic glasses [13], polymer hydrogels [14], supercooled liquids [15], Lennard-Jones glasses [16], silica glass [17]. It has been shown that non-affine deformations are responsible for viscoelasticity [12] and internal damping [18] of amorphous solids. The suppression of non-affine displacements leads to an enhancement of the local elastic moduli around nanoparticles of the host amorphous medium [19, 20].

The theoretical description of non-affine displacements is significantly complicated by the fact that continuum elasticity theory is not applicable at scales where non-affine deformations play a significant role [21]. As a result, the heterogeneity length scale ξ can be introduced, which separates large scales, where the continuum theory

of elasticity applies, and microscopic scales with significant non-affine deformations. The heterogeneity length scale depends on the strength of the disorder in the system and can be up to tens of interatomic distances [22].

At present, the theory of non-affine displacements based on fluctuations of elastic moduli in the framework of the continuum elasticity theory is well developed. DiDonna and Lubensky [23] found analytically and numerically that the non-affine correlation function $\langle \mathbf{u}^{\text{naff}}(\mathbf{r}) \cdot \mathbf{u}^{\text{naff}}(0) \rangle$ has power-law decay r^{-1} for systems with dimension $d = 3$, and logarithmic decay for $d = 2$. Such a decay was confirmed by Maloney *et al.* [24, 25] while examining the elastic response of two-dimensional Lennard-Jones glasses using computer simulations. The power-law correlations were also attributed to the elastic deformation field due to plastic events, which was substantiated by numerical simulations on hard-sphere glasses [26].

On the other hand, there is evidence that non-affine correlations decay exponentially in the elastic regime. Jana and Pastewka [13] studied correlations of non-affine displacements during simple shear deformation of Cu-Zr bulk metallic glasses in molecular dynamics calculations. Their calculations show an exponential correlation with a decay length, which they interpret as the size of a shear transformation zone in the elastic regime. Meenakshi and Gupta [27] demonstrate that the correlation function changes from exponential to the power-law decay at the yielding transition. Therefore, the debate about the power-law or exponential decay of the correlations of non-affine displacement fields is still unresolved.

Thus, the development of the theory of non-affine deformations is of great interest. The most important aspect is to take into account the heterogeneity length scale and to develop a theory that would be applicable on scales smaller than the heterogeneity length scale, which can reveal the exponential behavior of nonaffine deformations. At the heterogeneity length scale, the fluctuations of the elastic moduli are comparable to the mean elastic moduli. This not only prevents the application of continuum elasticity theory, but also raises an important issue about the mechanical stability of the disordered system.

* ybeltukov@gmail.com

When a system is cooled from the melt to temperatures well below the glass transition temperature, it reaches a metastable equilibrium, settling into one of many local minima of potential energy, thereby becoming an amorphous solid [12, 28]. Therefore, the disorder in an amorphous solid is constrained by the fact that such systems are stable, implying significant correlations of the force constants [11, 29]. It has been shown that the theory of positive-definite correlated random matrices is an effective way of accounting for the strong disorder that provides mechanical stability [30, 31].

Random matrix theory has been applied to study the mechanical properties of amorphous glassy materials and amorphous polymers [20, 30–34]. Random matrix theory has also been applied to jammed solids, which are widely studied nowadays [35–37]. Among the various random matrix ensembles, the Wishart ensemble is crucial for examining the characteristics of strongly disordered stable mechanical systems, as it involves positive semidefinite random matrices. In particular, the correlated Wishart ensemble allowed us to derive the analytical form of the boson peak and the dynamical structure factor [30, 31], describe the Ioffe-Regel crossover and the viscoelastic properties [38]. It also explains the enhancement of the local elastic moduli due to the suppression of the non-affine deformations in the interfacial region around nanoparticles in an amorphous host material, which may significantly increase the macroscopic stiffness of nanocomposites [19, 20]. The obtained thickness of the interfacial region depends on the strength of the disorder and is determined by the heterogeneity length scale ξ , which is of the same order as the length scale of the boson peak. This suggests that random matrix theory is a valuable analytical method for capturing the universal properties of amorphous solids.

In this work, we present a theoretical study of non-affine elastic response correlation properties using the theory of positive-definite correlated random matrices and compare them to the results of the molecular dynamics simulation of polystyrene on the amorphous state. Section II defines the main concepts and the averaging procedure for obtaining the covariance of non-affine displacements. In Section III, the random matrix theory is applied to find the general form of the covariance of non-affine deformations. In Section IV, the case of an amorphous medium with homogeneous statistical properties is considered. In Section V, the case of strong disorder is considered, and the main results for the correlation properties of the divergence and the rotor of the non-affine displacement field are obtained. In Section VI, the theoretical results are compared to the molecular dynamics simulation of polystyrene in the amorphous state. Finally, the results obtained are discussed in Section VII.

II. AFFINE AND NON-AFFINE DISPLACEMENTS

In this paper, we explore the mechanical behavior of an amorphous solid that has been quenched to zero temperature, allowing it to reach a local potential energy minimum. In the absence of thermal fluctuations, the system can persist in this state for an extended period. When external forces \mathbf{f}_i are applied at a frequency ω , they induce particle displacements \mathbf{u}_i from their equilibrium positions. We consider small external forces, ensuring that the quenched system stays near the local equilibrium without transitioning to other potential energy minima. In the linear approximation, the elastic response \mathbf{u}_i is defined by the following system of linear equations:

$$\sum_{j\beta} [\Phi_{i\alpha,j\beta} - \omega^2 m_{i\alpha,j\beta}] u_{j\beta} = f_{i\alpha}, \quad (1)$$

where $\hat{\Phi}$ is the force constant matrix and \hat{m} is the mass matrix. The indices i and j enumerate the atoms in the system ($1 \dots N$), while α and β denote the Cartesian indices (x, y, z for $d = 3$ or x, y for $d = 2$) of the corresponding atoms. The elements of the force-constant matrix $\hat{\Phi}$ are defined by the Hessian of the total potential energy U

$$\Phi_{i\alpha,j\beta} = \left. \frac{\partial^2 U(\mathbf{r}_1, \mathbf{r}_2, \dots, \mathbf{r}_N)}{\partial r_{i\alpha} \partial r_{j\beta}} \right|_{\mathbf{r}_i = \mathbf{r}_i^{\text{eq}}} \quad (2)$$

taken at the equilibrium atomic coordinates \mathbf{r}_i^{eq} . The mass matrix \hat{m} is the Hessian of the kinetic energy with respect to velocities, specifically $m_{i\alpha,j\beta} = m_i \delta_{ij} \delta_{\alpha\beta}$ for the atomic system under consideration. Utilizing Eq. (1), the atomic displacements can be explicitly expressed as

$$u_{i\alpha} = \sum_{j\beta} \left(\frac{1}{\hat{\Phi} - \omega^2 \hat{m}} \right)_{i\alpha,j\beta} f_{j\beta}. \quad (3)$$

Matrices $\hat{\Phi}$ and \hat{m} have the size $N_{\text{dof}} \times N_{\text{dof}}$, where $N_{\text{dof}} = dN$ is the number of degrees of freedom. However, in the amorphous systems under consideration, there are some number N_{triv} of trivial degrees of freedom related to the free translation and rotation of the system without changing the potential energy (d and $d(d-1)/2$, respectively). Therefore, to simplify the analysis, the inversion of any $N_{\text{dof}} \times N_{\text{dof}}$ is assumed to be performed over the reduced subspace of non-trivial degrees of freedom $N'_{\text{dof}} = N_{\text{dof}} - N_{\text{triv}}$. This helps to exclude trivial degrees of freedom and avoid divergence caused by the system's acceleration, which might formally arise due to non-zero total forces as $\omega \rightarrow 0$.

The specific equilibrium coordinates $\mathbf{r}_1^{\text{eq}}, \mathbf{r}_2^{\text{eq}}, \dots, \mathbf{r}_N^{\text{eq}}$ depend on the cooling process of the melts forming the amorphous material. Therefore, the components of the force-constants matrix $\hat{\Phi}$ depend on the particular system under consideration and can vary in a broad range [11].

As a result, under an external uniform stress, not only macroscopic (affine) deformations occur, but also local

(non-affine) atomic displacements that depend on the degree of disorder. In this light, it is natural to represent the atomic displacement field as a sum of affine and non-affine components [23]:

$$u_{i\alpha} = u_{i\alpha}^{\text{aff}} + u_{i\alpha}^{\text{naff}}, \quad (4)$$

where the affine displacements are linearly defined by the macroscopic uniform strain tensor ε as follows:

$$u_{i\alpha}^{\text{aff}} = \sum_{\beta} \varepsilon_{\alpha\beta} r_{i\beta}^{\text{eq}}. \quad (5)$$

As non-affine deformations arise due to the system's disorder, it is reasonable to assume that their average across the ensemble of the disordered system equals zero.

Each realization of the amorphous medium gives different atomic positions \mathbf{r}_i^{eq} . Therefore, the direct averaging of atomic displacements over an ensemble of such amorphous systems is not really meaningful. Therefore, we introduce the concept of the reference lattice with nodes $\mathbf{r}_i^{\text{ref}}$ placed on a simple cubic lattice for $d = 3$ or a square lattice for $d = 2$. For the simplicity of the further analysis, we assume that the number of nodes is equal to the number of atoms N . Therefore, the average density of atoms n_{at} is equal to the density of the nodes. Now we can associate atomic displacements with displacements on the nodes:

$$u_{j\alpha}^{\text{ref}} = \sum_i u_{i\alpha} \phi_{ij}, \quad (6)$$

where $\hat{\phi}$ is some smoothing matrix satisfying the normalization condition $\sum_i \phi_{ij} = 1$ and the rule $\sum_i \phi_{ij} (\mathbf{r}_i - \mathbf{r}_j^{\text{ref}}) = 0$. The latter guarantees that displacements $u_{j\alpha}^{\text{ref}}$ are affine if the atomic displacements $u_{j\alpha}$ are affine. The further analysis weakly depends on the particular choice of $\hat{\phi}$. An example of such a smoothing matrix is provided in Section VI devoted to molecular dynamics.

At the same time, forces $f_{i\alpha}$ acting on atoms placed in some force field may also depend on their positions. Therefore, it is natural to define them using forces defined on the nodes $f_{j\alpha}^{\text{ref}}$, which do not depend on the specific equilibrium coordinates:

$$f_{i\alpha} = \sum_j \phi_{ij} f_{j\alpha}^{\text{ref}}, \quad (7)$$

where the same smoothing matrix $\hat{\phi}$ is used. Thus, we define the force-constant matrix and the mass matrix on the reference lattice as

$$\Phi_{i\alpha,j\beta}^{\text{ref}} = \sum_{i'j'} (\hat{\phi}^{-1})_{ii'} \Phi_{i'\alpha,j'\beta} (\hat{\phi}^{-1})_{j'j}, \quad (8)$$

$$m_{i\alpha,j\beta}^{\text{ref}} = \sum_{i'j'} (\hat{\phi}^{-1})_{ii'} m_{i'\alpha,j'\beta} (\hat{\phi}^{-1})_{j'j}. \quad (9)$$

Such definitions ensure the symmetry of the matrices $\hat{\Phi}^{\text{ref}}$ and \hat{m}^{ref} and fulfill the expected relationship

$$u_{i\alpha}^{\text{ref}} = \sum_{j\beta} \left(\frac{1}{\hat{\Phi}^{\text{ref}} - \omega^2 \hat{m}^{\text{ref}}} \right)_{i\alpha,j\beta} f_{j\beta}^{\text{ref}}. \quad (10)$$

According to Eq. (10), the average response $\langle u_{i\alpha}^{\text{ref}} \rangle$ can be written as:

$$\langle u_{i\alpha}^{\text{ref}} \rangle = \sum_{j\beta} G_{i\alpha,j\beta} f_{j\beta}^{\text{ref}}, \quad (11)$$

where the resolvent (also known as the Green function) is introduced:

$$\hat{G} = \left\langle \frac{1}{\hat{\Phi}^{\text{ref}} - \omega^2 \hat{m}^{\text{ref}}} \right\rangle. \quad (12)$$

Angular brackets denote the averaging over different realizations of the amorphous system. The resolvent \hat{G} is a regular matrix on a simple cubic (or square) lattice. For the further analysis of static elastic properties, we will use small imaginary frequency $\omega = i\epsilon$ with small positive $\epsilon \rightarrow 0$, which results in the positive-definite resolvent

$$\hat{G} = \left\langle \frac{1}{\hat{\Phi}^{\text{ref}} + \epsilon^2 \hat{m}^{\text{ref}}} \right\rangle. \quad (13)$$

For uniform stress, the average displacements of the reference nodes $\langle u_{i\alpha}^{\text{ref}} \rangle$ are affine:

$$\langle u_{i\alpha}^{\text{ref}} \rangle = \sum_{\beta} \varepsilon_{\alpha\beta} r_{i\beta}^{\text{ref}}. \quad (14)$$

Therefore, the non-affine displacements are the deviation from the mean displacement, $u_{i\alpha}^{\text{ref}} - \langle u_{i\alpha}^{\text{ref}} \rangle$. Thus, non-affine displacements have a zero mean but may possess nonzero correlations, which represent the correlation properties of the elastic response of an amorphous solid. The pairwise covariance of non-affine displacements is defined as

$$K_{i\alpha,j\beta} = \langle u_{i\alpha}^{\text{ref}} u_{j\beta}^{\text{ref}} \rangle - \langle u_{i\alpha}^{\text{ref}} \rangle \langle u_{j\beta}^{\text{ref}} \rangle. \quad (15)$$

In this paper, we firstly analyze the covariance matrix $K_{i\alpha,j\beta}$ for arbitrary (presumably smooth) force fields given by $f_{i\alpha}^{\text{ref}}$. Then, in the final steps, we will take into account the property (14) for the affine strain.

To facilitate a more concise notation for subsequent analysis, we substitute the combined indices $i\alpha$ and $j\beta$ with the simpler indices a and b , respectively. In this manner, the covariance of non-affine displacements can be written as follows:

$$K_{ab} = \langle u_a^{\text{ref}} u_b^{\text{ref}} \rangle - \langle u_a^{\text{ref}} \rangle \langle u_b^{\text{ref}} \rangle. \quad (16)$$

The average product of displacements can be written as

$$\langle u_a^{\text{ref}} u_b^{\text{ref}} \rangle = \sum_{a'b'} \mathcal{G}_{ab,a'b'} f_{a'}^{\text{ref}} f_{b'}^{\text{ref}}, \quad (17)$$

where the four-point resolvent (also known as the two-particle Green function) is introduced:

$$\mathcal{G}_{ab,a'b'} = \left\langle \left(\frac{1}{\hat{\Phi}^{\text{ref}} + \epsilon^2 \hat{m}^{\text{ref}}} \right)_{aa'} \left(\frac{1}{\hat{\Phi}^{\text{ref}} + \epsilon^2 \hat{m}^{\text{ref}}} \right)_{bb'} \right\rangle. \quad (18)$$

The primary objective of this paper is to examine the spatial properties of the covariance of non-affine displacements given by K_{ab} . To facilitate the averaging and derive \hat{G} and $\hat{\mathcal{G}}$, we employ techniques of the random matrix theory.

III. RANDOM MATRIX THEORY

A. Correlated Wishart ensemble

The essential aspect of employing random matrix theory in analyzing the mechanical properties of solids is ensuring their mechanical stability, which is represented by the force-constant matrix $\hat{\Phi}$ and consequently the matrix $\hat{\Phi}^{\text{ref}}$ being positive semidefinite. This implies that the total potential energy

$$U = \frac{1}{2} \sum_{ab} \Phi_{ab}^{\text{ref}} u_a^{\text{ref}} u_b^{\text{ref}} \quad (19)$$

remains non-negative for any atomic displacements u_a . There is also a permutation rule $\Phi_{ab} = \Phi_{ba}$ which follows from the definition of the force constant matrix (2). The above-mentioned conditions are equivalent to the possibility of representing the force-constant matrix as [30]:

$$\Phi_{ab}^{\text{ref}} = \sum_k A_{ak} A_{bk}, \quad (20)$$

which can be written as $\hat{\Phi}^{\text{ref}} = \hat{A} \cdot \hat{A}^T$, where the dot (\cdot) means the contraction over one inner index. The matrix \hat{A} in the relation (20) can be interpreted as it follows. Its index a enumerates degrees of freedom, while its index k enumerates bonds with the positive-definite quadratic potential energy

$$U_k = \frac{1}{2} (A_{ak} u_a^{\text{ref}})^2. \quad (21)$$

Each bond may involve several degrees of freedom, and the number and positions of non-zero elements in the matrix \hat{A} depend on the type of interaction between atoms in an amorphous solid [39]. Thus \hat{A} is a rectangular matrix of size $N_{\text{dof}} \times N_b$, where $N_{\text{dof}} = dN$ is the number of degrees of freedom, and N_b is the number of bonds. For the further analysis, we reserve indices a and b to enumerate degrees of freedom and indices k and l to enumerate bonds.

The presence of disorder in atomic arrangements leads to the random nature of the matrix \hat{A} . Therefore, to describe the amorphous state, one can assume that the non-zero matrix elements A_{ak} are random numbers. Following the paper [20], we consider the Gaussian random numbers A_{ak} with zero mean and covariance

$$\langle A_{ak} A_{bl} \rangle = C_{ab,kl}. \quad (22)$$

For such a random matrix \hat{A} , ensemble of matrices $\hat{\Phi}^{\text{ref}} = \hat{A} \cdot \hat{A}^T$ forms a correlated Wishart ensemble.

The covariance matrix \hat{C} as well as the two-particle Green function \hat{G} have four distinct indices. These matrices are referred to as four-point matrices, in accordance with the notation employed in [40]. In our paper, we use calligraphic letters and wide hats for four-point matrices to distinguish them from standard two-index matrices.

The covariance matrix \hat{C} plays a key role in describing the general properties of strongly disordered systems since it contains their main features. The structure of \hat{C} is affected by the fact that in real amorphous solids short-range interactions between atoms dominate over long-range interactions, so the covariance matrix \hat{C} has a sparse structure. At the same time, it has several important properties, which follow from the definition (22).

The covariance matrix \hat{C} has the property

$$\sum_{abkl} C_{ab,kl} B_{ak} B_{bl} = \langle \text{Tr}^2 [\hat{A} \cdot \hat{B}^T] \rangle \geq 0 \quad (23)$$

for any real matrix \hat{B} of size $N_{\text{dof}} \times N_b$. It follows that for any positive semidefinite matrix \hat{X} of size $N_b \times N_b$, the matrix $\hat{Y} = \hat{C} : \hat{X}$ of size $N_{\text{dof}} \times N_{\text{dof}}$ is also positive semidefinite, whereas the double contraction $(:)$ means the summation over two inner indices

$$Y_{ab} = \sum_{kl} C_{ab,kl} X_{kl}. \quad (24)$$

Indeed, any positive semidefinite matrix \hat{X} can be presented as $\hat{X} = \hat{Z} \cdot \hat{Z}^T$, and

$$\sum_{ab} x_a Y_{ab} x_b = \sum_m \sum_{abkl} x_a Z_{km} C_{ab,kl} Z_{lm} x_b \geq 0 \quad (25)$$

for any real x_a . Thus $\hat{X} \mapsto \hat{C} : \hat{X}$ is a linear map from matrices of size $N_b \times N_b$ to matrices of size $N_{\text{dof}} \times N_{\text{dof}}$, which preserves positive semidefiniteness. Using the same idea, one can show that for any positive semidefinite matrix \hat{Y} , the matrix $\hat{X} = \hat{C}^T : \hat{Y}$ is also positive semidefinite, where the transposition of the four-point matrix is the interchange of the left and the right pair of indices. Additionally, for any given pair of positive semidefinite matrices, denoted \hat{Y} and \hat{X} , the expression $\hat{Y} : \hat{C} : \hat{X}$ evaluates to a number that is guaranteed to be non-negative.

As demonstrated in [20] using the diagrammatic technique, the covariance matrix \hat{C} determines the resolvent \hat{G} defined in Eq. (13) by the coupled Dyson-Schwinger equations:

$$\hat{G} = \frac{1}{\hat{C} : \hat{G}^b + \epsilon^2 \hat{m}^{\text{ref}}}, \quad (26)$$

$$\hat{G}^b = \frac{1}{\hat{C}^T : \hat{G} + \hat{1}}, \quad (27)$$

where \hat{G}^b represents the secondary resolvent of the size $N_b \times N_b$:

$$\hat{G}^b = \left\langle \frac{1}{\hat{A}^T \frac{1}{\epsilon^2 \hat{m}^{\text{ref}}} \hat{A} + \hat{1}} \right\rangle. \quad (28)$$

In Eqs. (26) and (27) we have neglected the fluctuations in the mass matrix, $\hat{m}^{\text{ref}} = \langle \hat{m}^{\text{ref}} \rangle$. This is primarily

because our focus is on the static limit $\epsilon \rightarrow 0$. Additionally, mass disorder is typically less significant compared to force-constant disorder.

Equations (26) and (27) form a system of nonlinear equations. This naturally raises a question regarding whether a solution to the system indeed exists and, if it does, whether such a solution is unique. The physical solution corresponds to the positive semidefinite resolvent \hat{G} for $\epsilon > 0$. Since the covariance matrix \hat{C} as well as the matrix inversion preserve positive semidefiniteness, the matrix \hat{G}^b is also positive semidefinite.

Using the block-diagonal resolvent $\hat{G}_{bd} = \begin{pmatrix} \hat{G} & 0 \\ 0 & \hat{G}^b \end{pmatrix}$, one can write Eqs. (26) and (27) as one Dyson-Schwinger equation

$$\hat{G}_{bd} = \frac{1}{\hat{C}_{bd} : \hat{G}_{bd} + \hat{V}_{bd}}, \quad (29)$$

where

$$\hat{C}_{bd} : \begin{pmatrix} \hat{G} & 0 \\ 0 & \hat{G}^b \end{pmatrix} = \begin{pmatrix} \hat{C} : \hat{G}^b & 0 \\ 0 & \hat{C}^T : \hat{G} \end{pmatrix}, \quad \hat{V}_{bd} = \begin{pmatrix} \epsilon^2 \hat{m} & 0 \\ 0 & \hat{1} \end{pmatrix}. \quad (30)$$

The four-point matrix \hat{C}_{bd} preserves positive-semidefiniteness, and the matrices \hat{G}_{bd} and \hat{V}_{bd} are positive-definite. It is known that there is one and only one solution of Eq. (29) in the domain of positive-definite matrices [41]. In order to obtain the solution, one can use the simple iteration procedure. In terms of the resolvent \hat{G} , this iteration writes

$$\hat{G}_{n+1} = \left(\hat{C} : (\hat{C}^T : \hat{G}_n + \hat{1})^{-1} + \epsilon^2 \hat{m}^{\text{ref}} \right)^{-1}. \quad (31)$$

It converges to the solution, $\lim_{n \rightarrow \infty} \hat{G}_n = \hat{G}$, for any starting resolvent \hat{G}_0 being a positive-semidefinite matrix [41].

B. Four-point resolvent

Employing the diagram method outlined in Appendix A, the four-point resolvent $\hat{\mathcal{G}}$ can be expressed as

$$\mathcal{G}_{ab,a'b'} = \mathcal{L}_{ab,a'b'} + \mathcal{L}_{ab',a'b} - \mathcal{R}_{ab,a'b'}, \quad (32)$$

where the four-point matrix $\hat{\mathcal{L}}$ is defined as the solution of the equation (known as the two-particle Dyson equation)

$$\hat{\mathcal{L}} = \hat{\mathcal{R}} + \hat{\mathcal{R}} : \hat{\mathcal{T}} : \hat{\mathcal{L}}, \quad (33)$$

where

$$\mathcal{R}_{ab,a'b'} = G_{aa'} G_{bb'}, \quad (34)$$

$$\mathcal{T}_{ab,a'b'} = \sum_{klk'l'} \mathcal{C}_{ab,kl} G_{kk'}^b G_{ll'}^b \mathcal{C}_{a'b',k'l'}. \quad (35)$$

The first term in Eq. (32) corresponds to the ladder diagrams, while the second term corresponds to the twisted

diagrams. Accordingly, the covariance of the non-affine displacements can be written as

$$K_{ab} = K_{ab}^{\text{ld}} + K_{ab}^{\text{tw}}, \quad (36)$$

where the ladder term is

$$K_{ab}^{\text{ld}} = \sum_{a'b'} (\mathcal{L}_{ab,a'b'} - \mathcal{R}_{ab,a'b'}) f_{a'} f_{b'}, \quad (37)$$

and twisted term is

$$K_{ab}^{\text{tw}} = \sum_{a'b'} (\mathcal{L}_{ab',a'b} - \mathcal{R}_{ab,a'b'}) f_{a'} f_{b'}. \quad (38)$$

C. Four-point eigenvalue decomposition

Four-point matrices $\hat{\mathcal{R}}$ and $\hat{\mathcal{T}}$ are symmetric with respect to the transposition of the left and right pair of indices, $\hat{\mathcal{R}} = \hat{\mathcal{R}}^T$, $\hat{\mathcal{T}} = \hat{\mathcal{T}}^T$. At the same time, they are semidefinite with respect to the double contraction:

$$\hat{X} : \hat{\mathcal{R}} : \hat{X} \geq 0, \quad \hat{X} : \hat{\mathcal{T}} : \hat{X} \geq 0 \quad (39)$$

for any matrix \hat{X} , which follows from the definitions (34) and (35). Such positive semidefinite self-adjoint linear operators acting on matrices can be examined through the eigenvalue analysis. One can find N_{dof}^2 eigenvalues $\theta_v \geq 0$ such that

$$\hat{\mathcal{T}} : \hat{\mathcal{R}} : \hat{S}^{(v)} = \theta_v \hat{S}^{(v)}, \quad (40)$$

where $\hat{S}^{(v)}$ are the basis matrices (also known as the eigenmatrices [42]), which are orthonormal with the weight $\hat{\mathcal{R}}$ in the following sense

$$\hat{S}^{(v)} : \hat{\mathcal{R}} : \hat{S}^{(v')\dagger} \equiv \text{Tr}[\hat{S}^{(v)} \cdot \hat{\mathcal{R}} \cdot \hat{S}^{(v')\dagger}] = N'_{\text{dof}} \delta_{vv'}. \quad (41)$$

The Hermitian conjugation (\dagger) is employed in order to use the complex basis $\hat{S}^{(v)}$. Although real four-point matrices $\hat{\mathcal{T}}$ and $\hat{\mathcal{R}}$ allow for a real basis, the complex basis is chosen to enable further application of Fourier analysis.

At the same time, one can write the four-point matrices $\hat{\mathcal{T}}$ and $\hat{\mathcal{R}}$ as

$$\mathcal{T}_{ab,a'b'} = \sum_v \mathcal{S}_{ab}^{(v)} \theta_v \mathcal{S}_{a'b'}^{(v)\dagger}, \quad (42)$$

$$\mathcal{R}_{ab,a'b'} = \sum_v (\hat{G} \cdot \hat{S}^{(v)} \cdot \hat{G})_{ab} (\hat{G} \cdot \hat{S}^{(v)\dagger} \cdot \hat{G})_{a'b'}. \quad (43)$$

Consequently, the ladder four-point matrix $\hat{\mathcal{L}}$ is derived through the eigenvalue decomposition (42):

$$\mathcal{L}_{ab,a'b'} = \sum_v (\hat{G} \cdot \hat{S}^{(v)} \cdot \hat{G})_{ab} \frac{1}{1 - \theta_v} (\hat{G} \cdot \hat{S}^{(v)\dagger} \cdot \hat{G})_{a'b'}. \quad (44)$$

Thus, the non-affine displacement covariance K_{ab} has two components:

$$K_{ab}^{\text{ld}} = \sum_v (\hat{G} \cdot \hat{S}^{(v)} \cdot \hat{G})_{ab} \frac{\theta_v}{1 - \theta_v} (u \cdot \hat{S}^{(v)\dagger} \cdot u), \quad (45)$$

$$K_{ab}^{\text{tw}} = \sum_v (\hat{G} \cdot \hat{S}^{(v)} \cdot u)_a \frac{\theta_v}{1 - \theta_v} (u \cdot \hat{S}^{(v)\dagger} \cdot \hat{G})_b, \quad (46)$$

where u is a vector composed of N_{dof} elements $\langle u_a^{\text{ref}} \rangle$.

One can expect that θ_v could not exceed 1, which means the ladder four-point matrix $\hat{\mathcal{L}}$ is positive semidefinite. To elaborate on this question, one can consider the final convergence of the iteration (31). In this case, $\hat{G}_n = \hat{G} + d\hat{G}_n$ with small $d\hat{G}_n$. The next step of the iteration is $\hat{G}_{n+1} = \hat{G} + d\hat{G}_{n+1}$ with

$$d\hat{G}_{n+1} = \hat{\mathcal{R}} : \hat{\mathcal{T}} : d\hat{G}_n. \quad (47)$$

The iteration converges, which means that all eigenvalues of $\hat{\mathcal{R}} : \hat{\mathcal{T}}$ and $\hat{\mathcal{T}} : \hat{\mathcal{R}}$ are less than 1 for any $\epsilon > 0$. Therefore, $0 \leq \theta_v < 1$. At the same time, some of the limiting values $\lim_{\epsilon \rightarrow 0} \theta_v$ may be equal to 1.

For the further analysis, we assume that the correlation matrix $\hat{\mathcal{C}}$ is such that for any positive definite matrices \hat{X} and \hat{Y} , the matrices $\hat{\mathcal{C}} : \hat{X}$ and $\hat{\mathcal{C}}^T : \hat{Y}$ are strictly positive-definite, excluding N_{triv} trivial degrees of freedom. This assumption is essential and posits that the disorder introduced by the correlation matrix $\hat{\mathcal{C}}$ influences all N'_{dof} non-trivial degrees of freedom and all N_b bonds (at the same time, the matrix $\hat{\mathcal{C}}$ may be highly sparse). In this case, the map $\hat{X} \mapsto \hat{\mathcal{T}} : \hat{\mathcal{R}} : \hat{X}$ preserves the positive-definiteness of the matrix \hat{X} in the subspace of nontrivial degrees of freedom. For such maps, which preserve the cone of positive-definiteness, the Perron–Frobenius theorem is applicable [42]. It implies that the largest eigenvalue, denoted by θ_0 , is non-degenerate and the corresponding basis matrix $\hat{S}^{(0)}$ can be chosen to be positive semidefinite, having N'_{dof} positive eigenvalues and N_{triv} zero eigenvalues.

Taking the inverse of the Dyson-Schwinger equations (26), (27), and multiplying them by \hat{G} and \hat{G}^b with the double contraction, we obtain

$$\hat{G} : \hat{\mathcal{C}} : \hat{G}^b + \epsilon^2(\hat{G} : \hat{m}) = N'_{\text{dof}}, \quad (48)$$

$$\hat{G}^b : \hat{\mathcal{C}}^T : \hat{G} + \text{Tr}[\hat{G}^b] = N_b, \quad (49)$$

where we have taken into account that $\hat{G} : \hat{G}^{-1} = N'_{\text{dof}}$ due to exclusion of N_{triv} trivial degrees of freedom from the inversion. The difference of the above equations gives

$$\text{Tr}[\hat{G}^b] = N_b - N'_{\text{dof}} + \epsilon^2(\hat{G} : \hat{m}). \quad (50)$$

If $N_b > N'_{\text{dof}}$, $\text{Tr}[\hat{G}^b] = N_b - N'_{\text{dof}}$ as $\epsilon \rightarrow 0$. So the mean of eigenvalues of \hat{G}^b is equal to

$$\varkappa = 1 - N'_{\text{dof}}/N_b. \quad (51)$$

There is no critical behavior in this case unless $\varkappa \ll 1$, which will be considered further.

The case of $N_b < N'_{\text{dof}}$ is drastically different. The matrices \hat{G} , \hat{G}^b , and \hat{m} are positive semidefinite. Consequently, $\text{Tr}[\hat{G}^b]$ and $(\hat{G} : \hat{m})$ cannot be negative. As such, the value of $(\hat{G} : \hat{m})$ diverges proportionally to ϵ^{-2} . Hence, according to the Dyson-Schwinger equations (26)–(27), the resolvents scale as $\hat{G} \sim \epsilon^{-2}$ and $\hat{G}^b \sim \epsilon^2$. Such

resolvents correspond to a very loose system with an insufficient number of bonds, which we will not consider further.

Of greater interest is the case of a critical system when $N_b = N'_{\text{dof}}$. In this case, $\text{Tr}[\hat{G}^b] = \epsilon^2(\hat{G} : \hat{m})$ and the resolvents scale as $\hat{G} \sim \epsilon^{-1}$ and $\hat{G}^b \sim \epsilon$ according to the Dyson-Schwinger equations (26)–(27). For such a scaling, the Dyson-Schwinger equation reduces to $\hat{G} = (\hat{\mathcal{C}} : (\hat{\mathcal{C}}^T : \hat{G})^{-1})^{-1}$. Due to the ability of this equation to multiply \hat{G} by any scaling factor, there exists the basis matrix $\hat{S}^{(0)}$, which approaches \hat{G}^{-1} as $\epsilon \rightarrow 0$, and the corresponding eigenvalue θ_0 , which approaches 1. Using \hat{G}^{-1} as the first approximation of the basis matrix $\hat{S}^{(0)}$, the eigenvalue θ_0 can be estimated using Eq. (40) and the orthogonality relation (41) as

$$\theta_0 \approx \frac{\hat{G}^{-1} : \hat{\mathcal{R}} : \hat{\mathcal{T}} : \hat{\mathcal{R}} : \hat{G}^{-1}}{\hat{G}^{-1} : \hat{\mathcal{R}} : \hat{G}^{-1}}. \quad (52)$$

Using the properties $\hat{\mathcal{R}} : \hat{G}^{-1} = \hat{G}$, $\hat{\mathcal{C}}^T : \hat{G} = (\hat{G}^b)^{-1} - \hat{1}$, and the definition of the matrix $\hat{\mathcal{T}}$ given by Eq. (35), the eigenvalue is

$$\theta_0 \approx \frac{\text{Tr}[(\hat{1} - \hat{G}^b)^2]}{N'_{\text{dof}}} \approx 1 - 2 \frac{\text{Tr}[\hat{G}^b]}{N'_{\text{dof}}}. \quad (53)$$

Therefore, the eigenvalue θ_0 is close to 1 and $1 - \theta_0 \sim \epsilon$.

Behavior of the near-critical system with $0 < \varkappa \ll 1$ is similar to the critical system with finite ϵ . If the correlation properties of the disorder are sufficiently homogeneous, the maximum eigenvalue of \hat{G}^b is of the order of the mean eigenvalue \varkappa . Consequently, one can expect that all scaling properties for the critical system remain valid when ϵ is replaced by \varkappa :

$$\|\hat{G}\| \sim \varkappa^{-1}, \quad \|\hat{G}^b\| \sim \varkappa, \quad 1 - \theta_0 \sim \varkappa. \quad (54)$$

Such scalings are based on the assumption that the disorder is evenly distributed over the degrees of freedom. In general, if some degrees of freedom have stronger disorder than others, the approximation $\hat{S}^{(0)} \approx \hat{G}^{-1}$ may be inaccurate. Our further analysis does not strictly rely on this approximation, but it can give an estimate for the properties of $\hat{S}^{(0)}$.

IV. AMORPHOUS MEDIUM WITH HOMOGENEOUS STATISTICAL PROPERTIES

In the previous Section, the general properties of the correlated Wishart ensemble are discussed. However, the properties of the mechanical system impose restrictions on the matrix \hat{A} . In this Section, the indices of degrees of freedom a and b are replaced back by the combined indices $i\alpha$ and $j\beta$, indicating that one atom has d degrees of freedom.

Since the total energy of the system U does not change when the system is translated or rotated as a whole, there

are the sum rules for the matrix \hat{A} . As it follows from the Eqs. (2), (20), the translational invariance when the whole system is shifted to a constant vector $u_{i\alpha} = u_\alpha$ leads to the sum rule

$$\sum_i A_{i\alpha,k} = 0 \quad (55)$$

for any Cartesian index α and the bond number k . When the system is rotated by an infinitesimal angle, the displacements of the atoms are expressed as $u_{i\alpha} = \sum_\beta \omega_{\alpha\beta} r_{i\beta}^{\text{ref}}$, where $\omega_{\alpha\beta}$ are elements of the infinitesimal rotation tensor [43]. Therefore, as it follows from the Eqs. (2) and (20), the rotational invariance leads to the rule

$$\sum_i \epsilon_{\alpha\beta\gamma} r_{i\beta}^{\text{ref}} A_{i\alpha,k} = 0 \quad (56)$$

for any bond number k and Cartesian index γ , where $\epsilon_{\alpha\beta\gamma}$ is the Levi-Civita symbol.

The obtained relations for the matrix \hat{A} impose corresponding restrictions on the form of the correlation matrix \hat{C} :

$$\sum_i C_{i\alpha j\beta,kl} = \sum_j C_{i\alpha j\beta,kl} = 0, \quad (57)$$

$$\sum_i \epsilon_{\alpha\gamma\eta} r_{i\gamma}^{\text{ref}} C_{i\alpha j\beta,kl} = \sum_j \epsilon_{\beta\gamma\eta} r_{j\gamma}^{\text{ref}} C_{i\alpha j\beta,kl} = 0. \quad (58)$$

As a result, these sum rules are also applied for the four-point matrix $\mathcal{T}_{i\alpha j\beta, i'\alpha' j'\beta'}$ with the summation taken over any of the four indices i, j, i', j' .

As a result, all basis matrices also obey the given sum rules:

$$\sum_i S_{i\alpha j\beta}^{(v)} = \sum_j S_{i\alpha j\beta}^{(v)} = 0, \quad (59)$$

$$\sum_i \epsilon_{\alpha\gamma\eta} r_{i\gamma}^{\text{ref}} S_{i\alpha j\beta}^{(v)} = \sum_j \epsilon_{\beta\gamma\eta} r_{j\gamma}^{\text{ref}} S_{i\alpha j\beta}^{(v)} = 0. \quad (60)$$

The amorphous medium under consideration has homogeneous statistical properties. As a result, the resolvent $G_{i\alpha j\beta}$ depends only on the difference between coordinates $\mathbf{r}_i - \mathbf{r}_j$. Thus, it is worth defining the Green function as a Fourier transform of the resolvent

$$G_{\alpha\beta}(\mathbf{q}) = \frac{1}{N} \sum_{ij} G_{i\alpha j\beta} e^{i\mathbf{q} \cdot (\mathbf{r}_i^{\text{ref}} - \mathbf{r}_j^{\text{ref}})}. \quad (61)$$

Similarly, the Fourier transform of mean atomic displacements and forces is:

$$\langle u_\alpha^{\text{ref}} \rangle(\mathbf{q}) = \sum_i \langle u_{i\alpha}^{\text{ref}} \rangle e^{i\mathbf{q} \cdot \mathbf{r}_i^{\text{ref}}}, \quad (62)$$

$$f_\alpha^{\text{ref}}(\mathbf{q}) = \sum_i f_{i\alpha}^{\text{ref}} e^{i\mathbf{q} \cdot \mathbf{r}_i^{\text{ref}}}. \quad (63)$$

Therefore, Eq. (11) reads

$$\langle u_\alpha^{\text{ref}} \rangle(\mathbf{q}) = G_{\alpha\beta}(\mathbf{q}) f_\beta^{\text{ref}}(\mathbf{q}), \quad (64)$$

where the Einstein notation for Cartesian indices is employed. In the continuum limit ($q \ll 1/a_0$, where a_0 is the reference lattice constant), the Green function of an isotropic elastic medium is [44]

$$G_{\alpha\beta}(\mathbf{q}) = \frac{1}{\mu} \left(\frac{\delta_{\alpha\beta}}{q^2} - \frac{\lambda + \mu}{\lambda + 2\mu} \frac{q_\alpha q_\beta}{q^4} \right), \quad (65)$$

where λ and μ are Lamé moduli of the medium. They are related to other known elastic moduli such that μ is the shear modulus, $\lambda + \frac{2}{3}\mu$ is the bulk modulus, and $\lambda/(2\lambda + 2\mu)$ is the Poisson's ratio for $d = 3$. For $d = 2$, the relation is slightly different: μ is the shear modulus, $\lambda + \mu$ is the bulk modulus, and $\lambda/(\lambda + 2\mu)$ is the Poisson's ratio.

The backward relation between $f_\alpha^{\text{ref}}(\mathbf{q})$ and $\langle u_\beta^{\text{ref}} \rangle(\mathbf{q})$ is given by the inverse Green function, which is given by the tensor inversion of Eq. (65):

$$(G^{-1})_{\alpha\beta}(\mathbf{q}) = (\lambda + \mu)q_\alpha q_\beta + \mu\delta_{\alpha\beta}q^2. \quad (66)$$

For zero frequency, $\epsilon \rightarrow 0$, the inverse Green function $(G^{-1})_{\alpha\beta}(\mathbf{q})$ is nothing more than the Fourier transform of the effective force-constant matrix $\langle (\hat{\Phi}^{\text{ref}})^{-1} \rangle^{-1}$.

Due to the statistical homogeneity of the system, the shift $\mathbf{r}_i^{\text{ref}} \rightarrow \mathbf{r}_i^{\text{ref}} + \delta\mathbf{r}$ leaves the system unchanged, where $\delta\mathbf{r}$ is the vector connecting two arbitrary nodes of the reference lattice. Such a shift may only multiply the basis matrix $\hat{S}^{(v)}$ by some phase factor $e^{-i\mathbf{p} \cdot \delta\mathbf{r}}$, where the wavevector \mathbf{p} depends on the eigenvalue index v . As a result, for the given eigenvalue number v , the Fourier transform

$$\sum_{ij} S_{i\alpha j\beta}^{(v)} e^{i\mathbf{p}_1 \cdot (\mathbf{r}_i^{\text{ref}} - \mathbf{r}_j^{\text{ref}}) + i\mathbf{p}' \cdot (\mathbf{r}_i^{\text{ref}} + \mathbf{r}_j^{\text{ref}})/2} \quad (67)$$

is not identically equal to zero only if $\mathbf{p}' = \mathbf{p}$. Therefore, all the eigenvalues can be grouped by the wavevector \mathbf{p} , and there is a one-to-one correspondence between the index v and the pair $(n\mathbf{p})$, where n is the branch number. This property is analogous to the Bloch theorem [45]. So we can introduce $\theta_n(\mathbf{p}) = \theta_{(n\mathbf{p})}$ and

$$S_{\alpha\beta}^{(n)}(\mathbf{p}_1; \mathbf{p}) = \sum_{ij} S_{i\alpha j\beta}^{(n\mathbf{p})} e^{i\mathbf{p}_1 \cdot (\mathbf{r}_i^{\text{ref}} - \mathbf{r}_j^{\text{ref}}) + i\mathbf{p} \cdot (\mathbf{r}_i^{\text{ref}} + \mathbf{r}_j^{\text{ref}})/2}. \quad (68)$$

The branches $\theta_n(\mathbf{p})$ are illustrated in Fig. 1. According to the Perron–Frobenius theorem, the largest eigenvalue θ_0 is not degenerate. Therefore, it may correspond to $\mathbf{p} = 0$ only and $\theta_0(0) = \theta_0$. Otherwise, there are at least two identical eigenvalues, which correspond to \mathbf{p} and $-\mathbf{p}$. The Perron–Frobenius theorem is applicable also for the subspace of the operator $\hat{\mathcal{T}}$ given by $\mathbf{p} = 0$. Therefore, the upper branch $\theta_0(\mathbf{p})$ is not degenerate for $\mathbf{p} = 0$ and all other branches $\theta_n(\mathbf{p})$ are lower than $\theta_0(\mathbf{p})$ for $\mathbf{p} = 0$ and $n > 0$. At the same time, some of the branches $\theta_n(\mathbf{p})$ may be degenerate for $\mathbf{p} = 0$ for $n > 0$ as illustrated in Fig. 1.

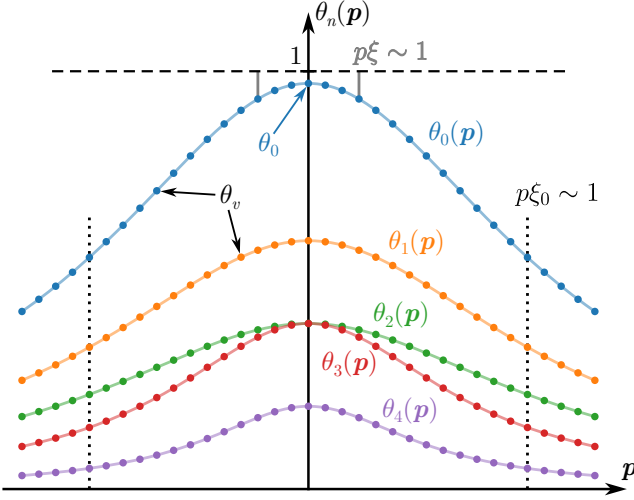


FIG. 1. Illustration of the bands $\theta_n(\mathbf{p})$ (color lines) and discrete eigenvalues θ_v for the finite system (color points) for $\tilde{\kappa} = 0.03$. Vertical gray lines show the position of $p\xi \sim 1$. The vertical dotted lines show the position of $p\xi_0 \sim 1$.

Given that $\langle u_{i\alpha}^{\text{ref}} \rangle$ represents the affine displacements $u_{i\alpha}^{\text{aff}}$ as described by Eq. (5), the covariance of non-affine deformation in the reciprocal space is

$$K_{\alpha\beta}(\mathbf{q}_1, \mathbf{q}_2) \equiv \sum_{ij} K_{i\alpha j\beta} e^{i\mathbf{q}_1 \cdot \mathbf{r}_i^{\text{ref}} - i\mathbf{q}_2 \cdot \mathbf{r}_j^{\text{ref}}} = K_{\alpha\beta}(\mathbf{q}_1) \delta(\mathbf{q}_1 - \mathbf{q}_2) \quad (69)$$

with

$$K_{\alpha\beta}(\mathbf{q}) = K_{\alpha\beta}^{\text{ld}}(\mathbf{q}) + K_{\alpha\beta}^{\text{tw}}(\mathbf{q}) \quad (70)$$

according to the ladder and twisted terms discussed in the previous Section. The ladder term has the form

$$K_{\alpha\beta}^{\text{ld}}(\mathbf{q}) = \sum_n h_n G_{\alpha\alpha'}(\mathbf{q}) S_{\alpha'\beta'}^{(n)}(\mathbf{q}; 0) G_{\beta'\beta}(\mathbf{q}), \quad (71)$$

where

$$h_n = \frac{\theta_n(0)}{1 - \theta_n(0)} \frac{\varepsilon_{\alpha\alpha'} \varepsilon_{\beta\beta'}}{4} \frac{\partial^2 S_{\alpha\beta}^{(n)}(\mathbf{q}; 0)}{\partial q_{\alpha'} \partial q_{\beta'}} \bigg|_{\mathbf{q}=0}. \quad (72)$$

The twisted term is

$$K_{\alpha\beta}^{\text{tw}}(\mathbf{q}) = \sum_n G_{\alpha\alpha'}(\mathbf{q}) F_{\alpha'}^{(n)}(\mathbf{q}) \frac{\theta_n(\mathbf{q})}{1 - \theta_n(\mathbf{q})} F_{\beta'}^{(n)*}(\mathbf{q}) G_{\beta'\beta}(\mathbf{q}), \quad (73)$$

where

$$F_{\alpha}^{(n)}(\mathbf{q}) = \varepsilon_{\beta\beta'} \frac{\partial S_{\alpha\beta}^{(n)}(\mathbf{q}/2 + \mathbf{q}_2; \mathbf{q})}{\partial q_{2\beta'}} \bigg|_{\mathbf{q}_2=0}. \quad (74)$$

V. STRONGLY DISORDERED MEDIUM

As was discussed at the end of Section III C, a strongly disordered amorphous medium corresponds to the case

$\varkappa \ll 1$. In this case, $\theta_0(0) = \theta_0$ is close to 1. All other branches $\theta_n(0)$ are lower than $\theta_0(0)$. Therefore, we can assume that in the general case, only the upper branch is close to 1 (see Fig. 1). Near $\mathbf{p} = 0$, it can be approximated as

$$\theta_0(\mathbf{p}) = 1 - \tilde{\kappa} - \xi_0^2 p^2 \quad (75)$$

with $\tilde{\kappa} \sim \varkappa \ll 1$. In the general case, the length scale ξ_0 does not contain any critical behavior and has a value of the order of the length scale of the atomic interaction, which is usually about the interatomic scale. The approximation (75) is applicable while $\xi_0 p \ll 1$, otherwise more terms are required.

For $\mathbf{p} = 0$, the tensor $S_{\alpha\beta}^{(0)}(\mathbf{p}_1; 0)$ is isotropic. Due to the sum rule (59), $S_{\alpha\beta}^{(0)}(\mathbf{q}; \mathbf{p})$ depends quadratically on \mathbf{q} for small \mathbf{q} and any \mathbf{p} . Therefore, up to the linear in \mathbf{p} terms, it is also isotropic:

$$S_{\alpha\beta}^{(0)}(\mathbf{q}; \mathbf{p}) = (\tilde{\lambda} + \tilde{\mu}) q_{\alpha} q_{\beta} + \tilde{\mu} \delta_{\alpha\beta} q^2 + \mathcal{O}(q^2 p^2), \quad (76)$$

where the parameters $\tilde{\lambda}$ and $\tilde{\mu}$ can be viewed as the disorder Lamé moduli. If the approximation $\hat{S}^{(0)} \approx \hat{G}^{-1}$ holds (see Section III C), the disorder moduli coincide with the elastic moduli: $\tilde{\mu} \approx \mu$ and $\tilde{\lambda} \approx \lambda$. As an example of such a case, in Appendix B a simple model of uncorrelated disorder is considered. However, we prefer to consider a more general case here.

As a result, the ladder term of the covariances is

$$K_{\alpha\beta}^{\text{ld}}(\mathbf{q}) = \frac{h_0}{q^4} \left(\frac{\tilde{\mu}}{\mu^2} (q^2 \delta_{\alpha\beta} - q_{\alpha} q_{\beta}) + \frac{\tilde{\lambda} + 2\tilde{\mu}}{(\lambda + 2\mu)^2} q_{\alpha} q_{\beta} \right), \quad (77)$$

where

$$h_0 = \frac{(\tilde{\lambda} + \tilde{\mu})(\varepsilon_{\gamma\gamma})^2 + (\tilde{\lambda} + 3\tilde{\mu})\varepsilon_{\gamma\eta}\varepsilon_{\eta\gamma}}{4\tilde{\kappa}}. \quad (78)$$

For the twisted term, we have

$$K_{\alpha\beta}^{\text{tw}}(\mathbf{q}) = \frac{G_{\alpha\alpha'}(\mathbf{q}) F_{\alpha'}^{(0)}(\mathbf{q}) F_{\beta'}^{(0)*}(\mathbf{q}) G_{\beta'\beta}(\mathbf{q})}{\tilde{\kappa}(1 + \xi^2 q^2)}, \quad (79)$$

where $\xi = \xi_0/\sqrt{\tilde{\kappa}}$ and

$$F_{\alpha}^{(0)}(\mathbf{q}) = \frac{\tilde{\lambda} + \tilde{\mu}}{2} q_{\alpha} \varepsilon_{\beta\beta} + \frac{\tilde{\lambda} + 3\tilde{\mu}}{2} \varepsilon_{\alpha\beta} q_{\beta}. \quad (80)$$

As \varkappa and $\tilde{\kappa}$ approach zero, the length scale ξ becomes indefinitely large, potentially surpassing all other length scales within the system, including the correlation length of the disorder.

The Fourier transform can be computed to determine the spatial correlations of non-affine displacements

$$K_{\alpha\beta}(\mathbf{r}) = \frac{1}{V_b} \int_{V_b} K_{\alpha\beta}(\mathbf{q}) e^{-i\mathbf{q}\mathbf{r}} d\mathbf{q} \quad (81)$$

with the integral taken over the first Brillouin zone of the reference lattice, where the volume of this zone is given

by $V_b = n_{\text{at}}(2\pi)^d$. Since $K_{\alpha\beta}(\mathbf{q}) = K_{\alpha\beta}^{\text{lad}}(\mathbf{q}) + K_{\alpha\beta}^{\text{tw}}(\mathbf{q})$, the Fourier transform (81) can be performed for both terms independently. For the ladder term given by Eq. 77 we obtain:

$$K_{\alpha\beta}^{\text{lad}}(\mathbf{r}) = -b_+ \delta_{\alpha\beta} \ln \frac{r}{r_0} + b_- \frac{r_\alpha r_\beta}{r^2}, \quad d = 2, \quad (82)$$

$$K_{\alpha\beta}^{\text{lad}}(\mathbf{r}) = b_+ \frac{\delta_{\alpha\beta}}{2r} + b_- \frac{r_\alpha r_\beta}{2r^3}, \quad d = 3, \quad (83)$$

where r_0 is the normalization length, which depends on the system size, and

$$b_\pm = \frac{h_0}{4\pi n_{\text{at}}} \left(\frac{\tilde{\mu}}{\mu^2} \pm \frac{\tilde{\lambda} + 2\tilde{\mu}}{(\lambda + 2\mu)^2} \right). \quad (84)$$

This power-law decay $K_{\alpha\beta}^{\text{lad}}(\mathbf{r}) \propto r^{2-d}$ is in agreement with the main results of the work [23] and has the same spatial behavior as the Green function of an isotropic elastic medium [44]. However, the power-law decay does not contain any specific length scale.

In contrast, the twisted term $K_{\alpha\beta}^{\text{tw}}(\mathbf{q})$ given by Eq. (79) has a non-trivial length scale ξ due to $1 + \xi^2 q^2$ in the denominator. The corresponding spatial correlation function $K_{\alpha\beta}^{\text{tw}}$ has exponential terms $\sim e^{-r/\xi}$ along with the power-law terms, while the expression is much lengthier and presented in Appendix C.

Thus, spatial correlations of non-affine displacements $K_{\alpha\beta}(\mathbf{r}) = \langle u_{\alpha}^{\text{naff}}(\mathbf{r}) u_{\beta}^{\text{naff}}(0) \rangle$ contain both power-law and exponential decay terms even in the case of uncorrelated disorder. In previous theoretical studies, to the best of our knowledge, the exponential decay was obtained for the correlated disorder only [23].

In reality, the derivatives of displacements usually play a more important role than the displacements themselves, since they represent the local strain. Therefore, we calculate the correlation function of the divergence of the non-affine displacement field, along with the correlation function of the rotor. Remarkably, our analysis shows that these functions have a simple analytical form.

A. Divergence

As a result of deformation, correlations between variations in the density of matter can occur in an amorphous system. This corresponds to the divergence correlator of non-affine displacements of the form

$$K_{\text{div}}(\mathbf{r}_i - \mathbf{r}_j) = \langle \text{div}(\mathbf{u}_i^{\text{naff}}) \text{div}(\mathbf{u}_j^{\text{naff}}) \rangle, \quad (85)$$

where the divergence of non-affine displacements on the reference lattice is defined as the corresponding finite difference. It is easy to see that the divergence correlator (85) is expressed by the correlator (15) in the following form:

$$K_{\text{div}}(\mathbf{r}_i - \mathbf{r}_j) = \frac{\partial^2 K_{\alpha\beta}(\mathbf{r}_i - \mathbf{r}_j)}{\partial r_{i\alpha} \partial r_{j\beta}}. \quad (86)$$

In the reciprocal space, it corresponds to

$$K_{\text{div}}(\mathbf{q}) = q_\alpha q_\beta K_{\alpha\beta}(\mathbf{q}). \quad (87)$$

For the volume deformation $\varepsilon_{\alpha\beta} = \varepsilon \delta_{\alpha\beta}$, we obtain

$$K_{\text{div}}(\mathbf{q}) = c_1 + \frac{c_2}{1 + \xi^2 q^2}, \quad (88)$$

where c_1 and c_2 are numerical factors of the order of $\varepsilon^2/\tilde{\kappa}$:

$$c_1 = \frac{d(d(\tilde{\lambda} + \tilde{\mu}) + \tilde{\lambda} + 3\tilde{\mu})(\tilde{\lambda} + 2\tilde{\mu})}{4\tilde{\kappa}(\lambda + 2\mu)^2} \varepsilon^2, \quad (89)$$

$$c_2 = \frac{(d(\tilde{\lambda} + \tilde{\mu}) + \tilde{\lambda} + 3\tilde{\mu})^2}{4\tilde{\kappa}(\lambda + 2\mu)^2} \varepsilon^2. \quad (90)$$

Taking the Fourier transform, we obtain

$$K_{\text{div}}(\mathbf{r}) = \frac{c_1}{n_{\text{at}}} \delta(\mathbf{r}) + \frac{c_2}{n_{\text{at}}} D(r) \quad (91)$$

with

$$D(r) = \frac{K_0(r/\xi)}{2\pi\xi^2}, \quad d = 2, \quad (92)$$

$$D(r) = \frac{e^{-r/\xi}}{4\pi r \xi^2}, \quad d = 3, \quad (93)$$

where $K_0(x)$ is the modified Bessel function of the second kind. In three dimensions, $D(r)$ has the explicit exponential decay given by Eq. (93), while in two dimensions, it has the asymptotic exponential behavior $D(r) = e^{-r/\xi}/\sqrt{8\pi r \xi^3}$ for $r \gg \xi$.

One can see that the classical power-law decay of the correlator $K_{\alpha\beta}(\mathbf{r})$ given by Eqs. (82)–(83) transforms to the delta function of the correlator of divergence $K_{\text{div}}(\mathbf{r})$ in Eq. (91). At the same time, the second term in Eq. (91) has the exponential decay at the length scale ξ , which follows from Eq. (79). Both terms have comparable integral contributions to $K_{\text{div}}(\mathbf{r})$ given by

$$\int K_{\text{div}}(\mathbf{r}) d\mathbf{r} = \frac{c_1 + c_2}{n_{\text{at}}} \sim \xi^2. \quad (94)$$

This integral is proportional to ξ^2 for any dimension d , which is in agreement with the works [46, 47].

For an arbitrary strain tensor $\boldsymbol{\varepsilon}$, the correlation function is anisotropic and has a lengthy expression given in Appendix C. However, the isotropic part of $K_{\text{div}}(\mathbf{r})$ has the same form as Eq. (91):

$$K_{\text{div}}^{\text{iso}}(\mathbf{r}) = \frac{c_1}{n_{\text{at}}} \delta(\mathbf{r}) + \frac{c_2}{n_{\text{at}}} D(r), \quad (95)$$

where the coefficients c_1 and c_2 for the general strain tensor $\boldsymbol{\varepsilon}$ are presented in Eqs. (C14) and (C18).

B. Rotor

One can also calculate the correlation function of the rotor of the non-affine displacement field

$$K_{\text{rot}}(\mathbf{r}_i - \mathbf{r}_j) = \langle \text{rot}(\mathbf{u}_i^{\text{naff}}) \cdot \text{rot}(\mathbf{u}_j^{\text{naff}}) \rangle, \quad (96)$$

which gives

$$K_{\text{rot}}(\mathbf{q}) = (q^2 \delta_{\alpha\beta} - q_\alpha q_\beta) K_{\alpha\beta}(\mathbf{q}). \quad (97)$$

For the volume deformation $\varepsilon_{\alpha\beta} = \varepsilon \delta_{\alpha\beta}$, we obtain

$$K_{\text{rot}}(\mathbf{q}) = c_3, \quad (98)$$

where c_3 is a numerical factor of the order of $\varepsilon^2/\tilde{\kappa}$:

$$c_3 = \frac{d(d-1)\tilde{\mu}(d(\tilde{\lambda} + \tilde{\mu}) + \tilde{\lambda} + 3\tilde{\mu})}{4\tilde{\kappa}\mu^2} \varepsilon^2. \quad (99)$$

As a result,

$$K_{\text{rot}}(\mathbf{r}) = \frac{c_3}{n_{\text{at}}} \delta(\mathbf{r}). \quad (100)$$

It is notable that the correlator of rotors does not contain the exponential decay in the case of volumetric deformation. In practice, the delta function is not precise and exhibits a broadening on the atomic scale. Furthermore, our analysis is limited to the upper branch $\theta_0(\mathbf{p})$. Nonetheless, certain lower branches might contribute a non-zero exponential term in $K_{\text{rot}}(\mathbf{r})$. These branches are not anticipated to exhibit critical behavior and similarly possess an atomic length scale. As a result, the proposed theory predicts that the correlation length for the rotor field is shorter than that for the divergence field, unexpectedly. This outcome will be verified in the next Section through molecular dynamics simulation of polystyrene.

For an arbitrary strain tensor ε , the correlation function $K_{\text{rot}}(\mathbf{q})$ had additional terms, which depend on \mathbf{q} , see Appendix C. Therefore, the isotropic part of $K_{\text{rot}}(\mathbf{r})$ has both the delta function and the additional exponential term in the general case:

$$K_{\text{rot}}^{\text{iso}}(\mathbf{r}) = \frac{c_3}{n_{\text{at}}} \delta(\mathbf{r}) + \frac{c_4}{n_{\text{at}}} D(r), \quad (101)$$

where the coefficients c_3 and c_4 for the general strain tensor ε are presented in Eqs. (C15) and (C19). The coefficient c_4 is equal to zero for the volumetric strain only.

VI. MOLECULAR DYNAMIC SIMULATIONS

In order to validate the theoretical findings, molecular dynamics simulations of a model atactic polystyrene in the amorphous state were conducted. The molecular dynamics simulations are performed using LAMMPS [48].

The MARTINI force-field is applied [19, 49], which represents each styrene monomer using four coarse-grained particles. Such a force-field is well-suited for large-scale simulations of polystyrene. A total of 240 chains, each consisting of 120 monomers, were simulated. Initially, the system was generated using random placement of polymer chains, each generated by the random monomer orientation. Then the system was briefly equilibrated at a high temperature of 2000 K for 10 ps. Subsequently, the system was quenched to zero temperature at a cooling rate of 100 K/ps. Finally, local equilibrium was achieved using the FIRE minimization method [50] ensuring that the residual forces do not exceed 10^{-9} kcal/(mol·nm). The simulation employed the NVT ensemble with a fixed density of $\rho = 0.95$ g/cm³ in a periodic simulation cell $17.0 \times 17.0 \times 17.0$ nm. An adaptive timestep was used during the simulation, with the maximum timestep limited to 10 fs.

Subsequently, two types of deformations were applied to the final system: volumetric and shear strains. For volumetric strain, the strain tensor is diagonal with diagonal elements $\varepsilon_{xx} = \varepsilon_{yy} = \varepsilon_{zz} = \varepsilon$. The shear deformation is represented by the traceless strain tensor ε . We selected it to be diagonal with diagonal elements $\varepsilon_{xx} = \varepsilon$ and $\varepsilon_{yy} = \varepsilon_{zz} = -\varepsilon/2$, allowing the use of an orthogonal simulation cell. In both cases, a small strain $\varepsilon = 10^{-5}$ is used to ensure the linear elastic regime. After the deformation of the simulation cell, the FIRE minimization method is used to minimize the energy again.

The obtained atomic displacements \mathbf{u}_i were mapped to the displacements on the reference lattice $\mathbf{u}_j^{\text{ref}}$ using Eq. (6) with the normalized smoothing matrix

$$\phi_{ij} = \tilde{\phi}_{ij} / \sum_{i'} \tilde{\phi}_{i'j}, \quad (102)$$

$$\tilde{\phi}_{ij} = \exp \left(-\frac{(\mathbf{r}_i^{\text{eq}} - \mathbf{r}_j^{\text{ref}})^2}{2w^2} \right). \quad (103)$$

The smoothing parameter w was varied between 0.2 and 0.6 nm. The non-affine correlation functions have been averaged over 100 independently quenched systems. Due to the presence of soft spots, a known phenomenon in amorphous solids [51–53], several of the generated systems have extraordinary non-affine displacements in such regions. If the largest atomic displacement exceeded the average modulus of atomic displacements by a factor of 100, the system was excluded from the averaging process to ensure the stability of the results.

The correlation function $K_{\alpha\alpha}(\mathbf{r}) = \langle u_{\alpha}^{\text{naff}}(\mathbf{r}) u_{\alpha}^{\text{naff}}(0) \rangle$ is plotted in Fig. 2 both for the volumetric strain and the shear. As was shown in the previous Section, the correlation function $K_{\alpha\alpha}(\mathbf{r})$ contains both exponential and power-law terms. For large distances r , one can expect the long-range power-law tail $1/r$. However, the limited system size does not allow to clearly observe such a dependence in Fig. 2.

The most interesting information is contained in the correlation functions for the divergence and the rotor of

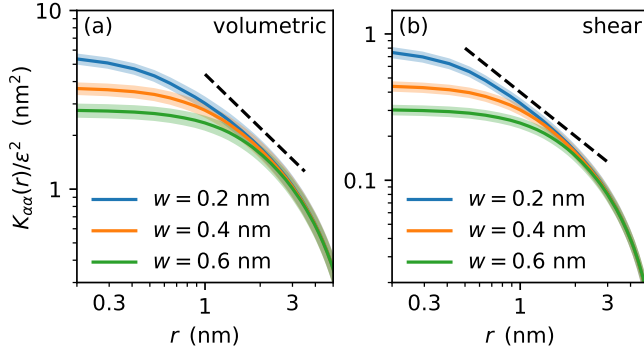


FIG. 2. Correlation function of the non-affine displacement field $K_{\alpha\alpha}(r)$ in model polystyrene system under volumetric strain (a) and shear strain (b) for different values of the smoothing parameter w . Shaded areas represent two standard deviations of the obtained data. Dashed lines represent the dependence $1/r$ as a visual guide.

the non-affine deformations, $K_{\text{div}}(\mathbf{r})$ and $K_{\text{rot}}(\mathbf{r})$. Therefore, the divergence and the rotor of the non-affine displacement field $\mathbf{u}_j^{\text{ref}}$ were computed using the finite-difference method. Then the corresponding correlation functions $K_{\text{div}}^{\text{iso}}(r)$ and $K_{\text{rot}}^{\text{iso}}(r)$ were obtained and averaged over different directions of \mathbf{r} and all the systems obtained.

Equation (91) states that $K_{\text{div}}(\mathbf{r})$ decays as $r^{-1}e^{-r/\xi}$ for large distances r . Therefore, we plot the normalized dimensionless correlation function $n_{\text{at}}rK_{\text{div}}^{\text{iso}}(r)/\varepsilon^2$ in Fig. 3(a) for the volumetric strain. It can be seen that after some transition at distances $r < 1$ nm, one can see an exponential decay $\sim \exp(-r/\xi)$ up to approximately $r = 6$ nm with $\xi = 1.4$ nm. Such a length scale is larger than the styrene monomer size, which is approximately 0.5 nm. At the same time, the length scale $\xi = 1.4$ nm coincides with the length scale of the increase in the elastic moduli around nanoparticles in the amorphous polymeric matrix, associated with the suppression of the non-affine displacements on the surface of nanoinclusions in a polymeric matrix [19, 20].

Using the same normalization, the correlation function for the rotor of non-affine displacements under volumetric strain, $K_{\text{rot}}^{\text{iso}}(r)$, is presented in Fig. 3(b). It demonstrates a much faster decay, which can be fitted by exponential decay $\sim \exp(-r/\xi_0)$ with a much shorter length scale $\xi_0 = 0.4$ nm, which is similar to the monomer size. Such a fast decay of $K_{\text{rot}}^{\text{iso}}(r)$ for volumetric strain fully corresponds to the theoretical predictions, which suggest that the term $\sim \exp(-r/\xi)$ with a long length scale ξ is vanishing in this case.

The correlation functions $K_{\text{div}}^{\text{iso}}(r)$ and $K_{\text{rot}}^{\text{iso}}(r)$ for the shear are plotted in Fig. 4. One can clearly observe the exponential decay $\sim \exp(-r/\xi)$ with $\xi \approx 1.4$ nm both for $K_{\text{div}}^{\text{iso}}(r)$ and $K_{\text{rot}}^{\text{iso}}(r)$ as predicted by the theory. A small value $3 \cdot 10^{-5}$ nm² has been added to $K_{\text{rot}}^{\text{iso}}(r)$ to compensate finite-size effects observed in the case of the shear strain.

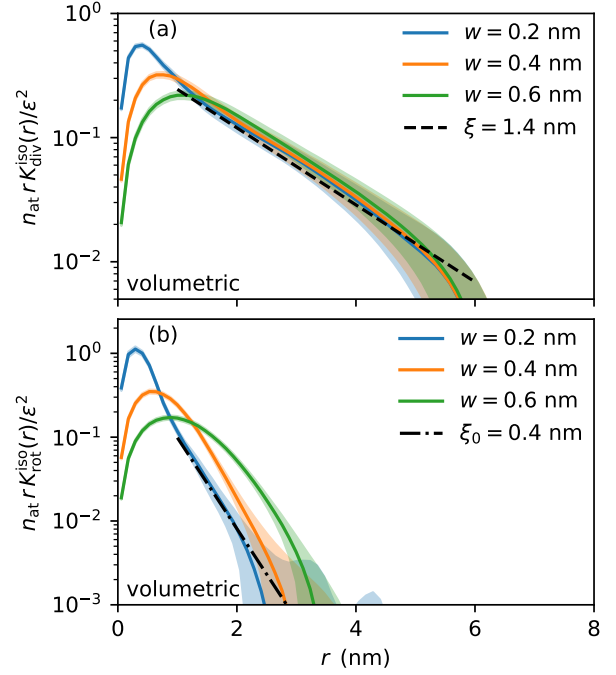


FIG. 3. Correlation function of the divergence (a) and the rotor (b) of the non-affine displacement field in model polystyrene under volumetric strain for different values of the smoothing parameter w . The normalization factor $n_{\text{at}}r/\varepsilon^2$ is used to plot the data. Shaded areas represent two standard deviations of the obtained data. Dashed and dash-dotted lines represent the dependencies $\exp(-r/\xi)$ and $\exp(-r/\xi_0)$, respectively.

VII. DISCUSSION

We consider the mechanical response of an amorphous solid quenched at zero temperature and at a local potential energy minimum. In the absence of thermal fluctuations, the system can remain in this state for a long time without external perturbations. We study the correlation of atomic non-affine displacements that occur under the action of a small external perturbation, so small that the quenched system remains in a local equilibrium position and does not reach other potential energy minima. For the molecular dynamics simulations we have performed, the values of the external strain are $\varepsilon = 10^{-5}$, ensuring the linear elastic regime.

To clarify the origin and nature of the non-affinity, we consider the correlated disorder of the quenched amorphous solid state by the methods of random matrix theory. The main point of the applied method is the requirement of mechanical stability of the disordered system, which corresponds to the positive semidefiniteness of the force constant matrix $\hat{\Phi}$ and its representation as a correlated Wishart ensemble $\hat{\Phi} = \hat{A} \cdot \hat{A}^T$ with a correlated random matrix \hat{A} . In amorphous solids, short-range atomic interactions typically prevail over long-range ones, resulting in a sparse covariance matrix $\hat{\mathcal{C}}$.

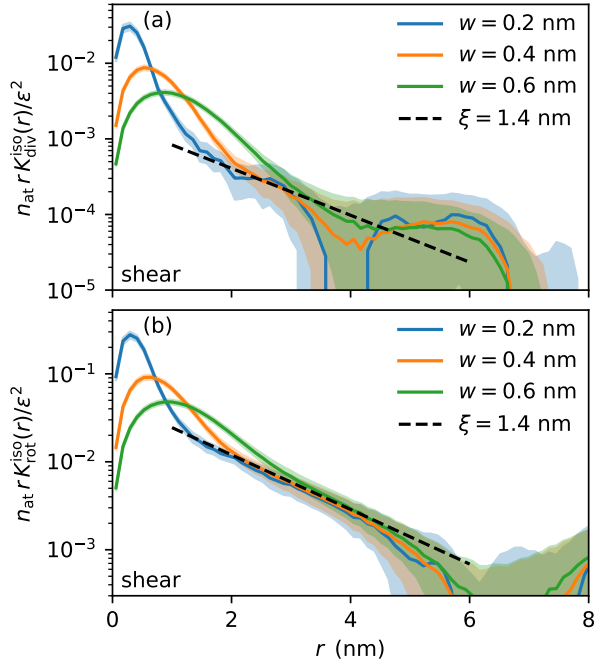


FIG. 4. Correlation function of the divergence (a) and the rotor (b) of the non-affine displacement field in model polystyrene under shear strain for different values of the smoothing parameter w . The normalization factor $n_{\text{at}} r / \epsilon^2$ is used to plot the data. Shaded areas represent two standard deviations of the obtained data. Dashed lines represent the dependency $\exp(-r/\xi)$.

Previously, the study of the statistical properties of the correlated Wishart ensemble helped us describe the well-known vibrational phenomena of amorphous solids, such as the boson peak and the Ioffe-Regel transition during the transformation of long-wavelength acoustic phonons into the diffusion type of vibrations [30, 31, 54]. It was shown that the frequencies of the Ioffe-Regel crossover and the boson peak have similar values, and the corresponding spatial scale, usually amounting to several nanometers, is associated with the strength of disorder and has the same order of magnitude as the non-affinity length scale ξ . The classical (continuum) theory of elasticity becomes inapplicable at such scales, since it is impossible to determine a smooth dependence of a displacement on the coordinate. In other words, length scale ξ separates macroscopic scales, to which the classical (continuum) theory of elasticity is applicable, and microscopic scales, on which the disorder of the system plays an essential role, which is consistent with the results of the paper [20, 31, 55] in the framework of the random matrix theory.

Using the diagram technique outlined in Appendix A, we find that the spatial correlations of the non-affine deformations $K_{\alpha\beta}(\mathbf{r}) = \langle u_{\alpha}^{\text{naff}}(\mathbf{r}) u_{\beta}^{\text{naff}}(0) \rangle$ have two terms, $K_{\alpha\beta}(\mathbf{r}) = K_{\alpha\beta}^{\text{ld}}(\mathbf{r}) + K_{\alpha\beta}^{\text{tw}}(\mathbf{r})$. The first term demonstrates the power-law decay $K_{\alpha\beta}^{\text{ld}}(\mathbf{r}) \propto r^{2-d}$, which has the same spatial behavior as the Green function of an isotropic

elastic medium [44]. This result is in exact agreement with the work of DiDonna and Lubensky [23], who proposed an analytic model for correlations in systems with a random distribution of elastic moduli, and was confirmed in the works [24–26, 56]. The second term demonstrates the exponential decay $K_{\alpha\beta}^{\text{tw}}(\mathbf{r}) \propto \exp(-r/\xi)$, expressing the large-scale correlation decreasing on the non-affinity length scale ξ . We guess that this exponentially decreasing contribution was marked in [13, 27]. Since $K_{\alpha\beta}(\mathbf{r})$ includes both exponential and power-law components, it is important to note that fitting this function with only the exponential or the power-law expression might lead to inconsistent outcomes.

Although the exponential correlation function for non-affine displacements was derived for correlated disorder with a specific correlation length [23], the current paper demonstrates the length scale ξ of the exponential decay depends on the disorder strength, and ξ could in theory surpass other relevant length scales in the system, such as interatomic distance, interaction distance, and the correlation length of the disorder.

An important result of our study is the analytical expression for the divergence $K_{\text{div}}(\mathbf{r}) = \langle \text{div} \mathbf{u}^{\text{naff}}(\mathbf{r}) \text{div} \mathbf{u}^{\text{naff}}(0) \rangle$ and rotor $K_{\text{rot}}(\mathbf{r}) = \langle \text{rot} \mathbf{u}^{\text{naff}}(\mathbf{r}) \cdot \text{rot} \mathbf{u}^{\text{naff}}(0) \rangle$ correlation functions of the non-affine displacement field. From a physical point of view, $K_{\text{div}}(\mathbf{r})$ corresponds to the correlation between the local fluctuations of the system density, and $K_{\text{rot}}(\mathbf{r})$ corresponds to the correlation between its local rotations. As was shown, $K_{\text{div}}(\mathbf{r})$ consists of two terms

$$K_{\text{div}}(\mathbf{r}) = A\delta(\mathbf{r}) + B \frac{e^{-r/\xi}}{r^{(d-1)/2}}, \quad (104)$$

where the delta-correlated component arises from the classical power-law decay of the correlation function $K_{\alpha\beta}^{\text{ld}}(\mathbf{r})$ and corresponds to white noise statistics, and the exponentially decaying correlation arises from heterogeneous length scale ξ .

The coefficients A and B depend on the Lamé moduli of the medium and on the macroscopic strain tensor. The theoretical dependence (88) is confirmed by molecular dynamics simulations of polystyrene. The corresponding heterogeneity length scale was estimated as $\xi \approx 1.4$ nm. Although the obtained length scale ξ is not particularly large in polystyrene, the calculations performed demonstrate the potential of such studies and pave the way for finding systems with even larger values of ξ .

At the same time, as it follows from our theoretical predictions (100), the rotor of the non-affine displacement field $K_{\text{rot}}(\mathbf{r})$ under volumetric deformation does not expose the large-scale correlations, but only the delta-correlated component. The molecular dynamics simulation confirms that in this particular case, $K_{\text{rot}}(\mathbf{r})$ has a rapid decay with the length scale $\xi_0 \ll \xi$.

The fact that the correlation functions $K_{\text{div}}(\mathbf{r})$ and $K_{\text{rot}}(\mathbf{r})$ do not contain power-law tails is caused by the perfect cancellation of such terms. In theory, the cancellation appears for the volumetric strain or for the

isotropic correlation functions $K_{\text{div}}^{\text{iso}}(\mathbf{r})$ and $K_{\text{rot}}^{\text{iso}}(\mathbf{r})$ in the case of the general strain tensor $\boldsymbol{\varepsilon}$. However, in real amorphous systems, the cancellation may not be perfect even in the mentioned cases. Therefore, the mentioned correlation functions have small additional power-law terms $\sim r^{-\gamma}$. Furthermore, in finite systems, finite-size effects significantly influence these power-law terms, hindering their cancellation. This complication can make the analysis of correlation functions more complex. This is why the rapidly quenched system was considered in the molecular dynamics study, which exhibits a large exponential contribution $\exp(-r/\xi)$ to the correlation functions. For the slowly relaxed system, the fitting using both the exponential decay and a small power-law tail is necessary.

The results of this study are of great importance for the physics of nanocomposites. It was previously shown that in a highly disordered medium with rigid inclusions of nanometer sizes, an effective rigid shell is formed around such nanoinclusions, for which the values of elastic modules exceed the values of volumetric elastic modules and depend on the degree of disorder [19, 20]. For example, calculations using the method of molecular dynamics of polystyrene with a silica nanoparticle show an increase in stiffness at a distance of about 1.4 nm around the nanoparticle [19]. At the same time, the scale that determines the thickness of such a shell exactly corresponds to the non-affinity length scale ξ obtained in this study. This results in the increase of the effective volume of nanoparticles and in the increase of their effect on the macroscopic elastic properties of nanocomposites, which is especially noticeable with similar values of the linear sizes of nanoparticles and the heterogeneity length scale ξ . At the same time, an exponential decrease of elastic modules near a rigid nanoparticle is observed, depending on the distance to it. This fact highlights the relationship between local elastic properties and non-affine deformations in systems with strong disorder. A similar behavior of elastic modules is observed near the transition between amorphous and crystalline layered structures [55]. The presence of transitional phases between structurally different regions is a manifestation of the heterogeneity of local deformations and is directly related to the disorder in such structures.

The results obtained are also important for the jammed solids [57, 58]. For such solids, a critical behavior is observed near the isostaticity point, where the number of bonds N_b is equal to the non-trivial degrees of freedom N'_{dof} . It corresponds to the small values of the parameter $\varkappa = 1 - N'_{\text{dof}}/N_b$. Therefore, the study of the correlation properties of the non-affine displacement field for jammed solids is of great interest. It can be compared to the proposed theory, expecting that the length scale ξ diverges near the isostaticity point.

For various disordered systems of arbitrary dimensionality, the heterogeneity length scale ξ can be estimated from the results of molecular dynamics calculations by plotting the dependence $K_{\text{div}}(\mathbf{r})$ and $K_{\text{rot}}(\mathbf{r})$, while the coefficients A and B in Eq. (104) can be used as fitting

parameters. Molecular dynamic modeling allows considering various amorphous and polymer systems, each of which can be characterized by its own non-affinity length scale ξ .

The relations obtained within the framework of the theory of random matrices can help to study the correlation properties of non-affine deformations at a nonzero frequency $\omega \neq 0$. This is especially relevant in the study of viscoelastic vibrational properties of amorphous systems. Additionally, exploring the correlation properties of non-affine deformations in the vicinity of interfaces between media possessing distinct elastic moduli is of significant interest, especially for nanocomposite amorphous systems. This subject remains a focus for further investigation.

VIII. CONCLUSION

In this paper, the theory of correlated random matrices is applied to analyze the correlation properties of non-affine deformations. The main contribution to the covariance matrix \hat{K} of non-affine displacements was obtained for a near-critical system. The proximity to the critical point is identified by the small parameter $\varkappa = 1 - N'_{\text{dof}}/N_b$. On the one hand, the parameter \varkappa is given by the ratio between the non-trivial degrees of freedom N'_{dof} and the number of bonds N_b , and it can be viewed as the deviation from the isostaticity point. On the other hand, the relative fluctuations of elastic properties grow as \varkappa decreases. Hence, the parameter \varkappa regulates the disorder, and a highly disordered system is represented by $\varkappa \rightarrow 0$.

It was shown that the correlation function of the divergence of non-affine displacements consists of a delta-correlated component (white noise) and exponentially decreasing large-scale correlations. The characteristic scale ξ , standing in the exponent, describes the heterogeneity length scale of the medium under study and diverges as $\varkappa^{-1/2}$ when $\varkappa \rightarrow 0$.

The correlation function of the rotor of the non-affine displacement field has also been calculated. For the volume macroscopic deformation, it consists only of a delta function broadened at the atomic length scale and does not include the large length scale ξ .

The molecular dynamics simulations of a model quenched polystyrene were performed to investigate the correlation properties of non-affine displacements. The results demonstrated that the divergence of these displacements matches theoretical predictions, exhibiting exponential decay with a length scale greater than the typical structural length scale ξ_0 . It was further demonstrated that the correlation function of the rotor of the non-affine displacement field for volumetric strain displays a rapid decay at a length scale ξ_0 , consistent with the proposed theory. At the same time, for the shear strain both $K_{\text{div}}(\mathbf{r})$ and $K_{\text{rot}}(\mathbf{r})$ have the same exponential decay $\exp(-r/\xi)$ with $\xi \gg \xi_0$.

IX. ACKNOWLEDGMENTS

Molecular dynamic simulations were supported by the Russian Science Foundation (grant no. #22-72-

10083, <https://rscf.ru/en/project/22-72-10083/>). The theoretical analysis was supported by the Theoretical Physics and Mathematics Advancement Foundation “Basis” (grant no. 24-1-2-36-1).

Appendix A: Random matrix theory: the averaging procedure

The averaging in the resolvent $\hat{G}(\omega) = \langle (\hat{\Phi} - \hat{m}\omega^2)^{-1} \rangle$ can be done analytically for $\hat{\Phi} = \hat{A}\hat{A}^T$ with a Gaussian random matrix \hat{A} . In the general case, the matrix elements are correlated: $\langle A_{ak}A_{bl} \rangle = C_{ab,kl}$. The resolvent $\hat{G}(\omega)$ can be presented as an infinite series

$$\hat{G}(\omega) = \left\langle \frac{1}{\hat{A}\hat{A}^T - \hat{m}\omega^2} \right\rangle = -\frac{1}{\hat{m}\omega^2} - \left\langle \frac{1}{\hat{m}\omega^2} \hat{A}\hat{A}^T \frac{1}{\hat{m}\omega^2} \right\rangle - \left\langle \frac{1}{\hat{m}\omega^2} \hat{A}\hat{A}^T \frac{1}{\hat{m}\omega^2} \hat{A}\hat{A}^T \frac{1}{\hat{m}\omega^2} \right\rangle - \dots \quad (\text{A1})$$

The elements of the resolvent $\hat{G}(\omega)$ can be written explicitly in the next form:

$$\begin{aligned} -G_{ab}(\omega) &= (\hat{m}\omega^2)_{ab}^{-1} + \sum_{a_1 a_2} \sum_{k_1 k_2} (\hat{m}\omega^2)_{aa_1}^{-1} \delta_{k_1 k_2} (\hat{m}\omega^2)_{b_1 b}^{-1} \langle A_{a_1 k_1} A_{k_2 a_2} \rangle \\ &+ \sum_{a_1 \dots a_4} \sum_{k_1 \dots k_4} (\hat{m}\omega^2)_{aa_1}^{-1} \delta_{k_1 k_2} (\hat{m}\omega^2)_{a_2 a_3}^{-1} \delta_{k_3 k_4} (\hat{m}\omega^2)_{a_4 b}^{-1} \langle A_{a_1 k_1} A_{a_2 k_2} A_{a_3 k_3} A_{a_4 k_4} \rangle + \dots \end{aligned} \quad (\text{A2})$$

We follow from the diagram technique described in [59] and introduce the next graphical representation:

$$(\hat{m}\omega^2)_{ab}^{-1} = \text{solid line } a \text{---} b, \quad \delta_{kl} = \text{dashed line } k \text{---} l, \quad \langle A_{i\alpha}^k A_{j\beta}^l \rangle = C_{i\alpha, j\beta}^{kl} = \text{double arc } a_k \text{---} l_b.$$

Here the solid line joining a and b is the factor $(\hat{m}\omega^2)_{ab}^{-1}$, the dashed line joining k and l is the Kronecker symbol δ_{kl} , and a painted joining ak and lb is the propagator $C_{ab,kl}$. Following these rules, the second term in (A2) corresponds to the next diagram:

$$\sum_{a_1 a_2} \sum_{k_1 k_2} (\hat{m}\omega^2)_{aa_1}^{-1} \delta_{k_1 k_2} (\hat{m}\omega^2)_{a_2 b}^{-1} \langle A_{a_1 k_1} A_{a_2 k_2} \rangle = \text{diagram with double arc } a_{k_1} \text{---} l_{b_1}.$$

Since the elements of the matrix \hat{A} are Gaussian random numbers, Wick's probability theorem is applicable for consecutively calculating even-point correlation functions, which are expressed as sums of all distinct products of two-point functions $\langle A_{a_1 k_1} A_{a_2 k_2} \rangle$. Therefore, a graphical representation of the resolvent $\hat{G}(\omega)$ is

$$\text{diagram with green blob } G = \text{solid line } a \text{---} b + \text{diagram with double arc } a_{k_1} \text{---} l_{b_1} + \text{diagram with two double arcs } a_{k_1} \text{---} l_{b_1} \text{ and } a_{k_2} \text{---} l_{b_2} + \dots \quad (\text{A3})$$

The presentation (A3) allows us to distinguish planar and non-planar diagrams. For planar diagrams, the number of closed loops (closed solid line or closed dashed line) is equal to the number of double arcs. For non-planar diagrams, the number of closed loops is less than the number of double arcs. Namely, the second diagram in (A3) is planar and contains one closed loop and one double arc, the third and fourth diagrams are planar and contain two closed loops and two double arcs, and the fifth diagram is non-planar and contains two double arcs and only one closed loop.

Each closed loop Λ corresponds to the calculation of a trace, which gives some factor T_Λ depending on the number of non-zero elements of the matrix \hat{A} . If each bond involves a sufficiently large number of degrees of freedom (although the matrix \hat{A} can be a highly sparse matrix), the factor $T_\Lambda \gg 1$ for each closed loop Λ . In the case of a sufficiently filled matrix \hat{A} , the factor $T_\Lambda \sim N$. At the condition $T_\Lambda \gg 1$, each planar diagram contributes much more than a non-planar diagram with the same number of double arcs. Therefore, we can exclude non-planar diagrams from the summation (A3) and take into account only planar diagrams.

Step-by-step solution for scalar model is described in [20], here we give only the final result:

$$\hat{G}(\omega) = \frac{1}{\hat{\mathcal{C}} : \hat{G}^b(\omega) - \hat{m}\omega^2}, \quad \hat{G}^b(\omega) = \frac{1}{\hat{\mathcal{C}}^T : \hat{G}(\omega) + \hat{1}}. \quad (\text{A4})$$

Taking into account (A2), we represent the four-point resolvent (18) as an infinite series:

$$\begin{aligned}
\mathcal{G}_{ab,a'b'} &= \left\langle \left(\frac{1}{\hat{\Phi} - \hat{m}\omega^2} \right)_{aa'} \left(\frac{1}{\hat{\Phi} - \hat{m}\omega^2} \right)_{bb'} \right\rangle = (\hat{m}\omega^2)_{aa'}^{-1} (\hat{m}\omega^2)_{bb'}^{-1} \\
&+ (\hat{m}\omega^2)_{aa'}^{-1} \sum_{b_1 b_2} \sum_{k_1 k_2} (\hat{m}\omega^2)_{bb_1}^{-1} \delta_{k_1 k_2} (\hat{m}\omega^2)_{b_2 b'}^{-1} \langle A_{b_1 k_1} A_{b_2 k_2} \rangle \\
&+ (\hat{m}\omega^2)_{bb'}^{-1} \sum_{a_1 a_2} \sum_{k_1 k_2} (\hat{m}\omega^2)_{aa_1}^{-1} \delta_{k_1 k_2} (\hat{m}\omega^2)_{a_2 a'}^{-1} \langle A_{a_1 k_1} A_{a_2 k_2} \rangle \\
&+ \sum_{a_1 a_2 b_1 b_2} \sum_{k_1 k_2 l_1 l_2} (\hat{m}\omega^2)_{aa_1}^{-1} \delta_{k_1 k_2} (\hat{m}\omega^2)_{a_2 a'}^{-1} (\hat{m}\omega^2)_{bb_1}^{-1} \delta_{l_1 l_2} (\hat{m}\omega^2)_{b_2 b'}^{-1} \langle A_{a_1 k_1} A_{a_2 k_2} A_{b_1 l_1} A_{b_2 l_2} \rangle + \dots \quad (A5)
\end{aligned}$$

Using the same graphical representation, we place diagrams of the first multiplier above the second one. Therefore, following Wick's probability theorem, we can express Eq. (A5) in diagrams as:

$$\mathcal{G}_{ab,a'b'} = \begin{array}{c} \text{diagram 1} \\ \text{diagram 2} \\ \text{diagram 3} \\ \text{diagram 4} \\ \text{diagram 5} \\ \text{diagram 6} \end{array} + \dots \quad (A6)$$

In Eq. (A6) can be seen that diagrams with painted joining between upper and lower ones have one closed loop less than similar ones of the $G_{aa'} G_{bb'}$. The diagrams that follow these two from Eq. (A6) can be obtained from them in a similar way to the previous case \hat{G} . It is not difficult to see that when increasing the number of connections from the upper diagrams to the lower ones, a certain pattern must be followed so that the number of closed loops is one less than in $G_{aa'} G_{bb'}$:

$$\begin{array}{c} \text{diagram 1} \\ \text{diagram 2} \end{array} \quad (A7)$$

The presentation (A7) allows us to distinguish stair and twisted diagrams. Note that by rearranging the indices of the lower or upper diagram, the first type can be obtained from the second, and vice versa. Therefore, we only need to keep track of one type of diagrams.

As the structure of ladder diagrams is simpler, we will focus on this type of diagram. As can be seen from (A7), any other ladder diagram can be connected to any ladder diagram on either the left or right side and we will get a diagram of the same type. Then, considering all possible variants of the upper and lower diagrams, we get a graphical representation of the sum of all ladder diagrams:

$$\begin{array}{c} \text{diagram 1} \\ \text{diagram 2} \\ \text{diagram 3} \\ \text{diagram 4} \\ \text{diagram 5} \end{array} = \begin{array}{c} \text{diagram 6} \\ \text{diagram 7} \\ \text{diagram 8} \\ \text{diagram 9} \\ \text{diagram 10} \end{array} \quad (A8)$$

Thus, the four-point resolvent (18) can be written as it follows:

$$\mathcal{G}_{ab,a'b'} = \mathcal{L}_{ab,a'b'} + \mathcal{L}_{ab',a'b} - G_{aa'} G_{b'b}, \quad (A9)$$

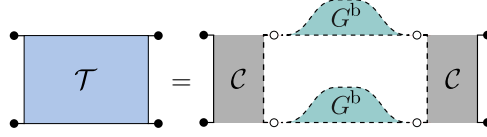
where the term $\mathcal{L}_{ab,a'b'}$ represents the contribution of ladder diagrams, and the term $\mathcal{L}_{ab',a'b}$ represents the contribution of twisted diagrams. As it follows from the diagram (A8), $\mathcal{L}_{ab,a'b'}$ can be written as

$$\begin{array}{c} \text{diagram 1} \\ \text{diagram 2} \\ \text{diagram 3} \\ \text{diagram 4} \end{array} = \begin{array}{c} \text{diagram 5} \\ \text{diagram 6} \\ \text{diagram 7} \\ \text{diagram 8} \end{array}, \quad (A10)$$

where we introduced $\hat{\mathcal{R}}$ as

$$\begin{array}{c} \text{diagram 1} \\ \text{diagram 2} \end{array} = \begin{array}{c} \text{diagram 3} \\ \text{diagram 4} \end{array}, \quad \text{or} \quad \mathcal{R}_{ab,a'b'} = G_{aa'} G_{b'b}, \quad (A11)$$

and we defined $\hat{\mathcal{T}}$ as



$$\mathcal{T} = \mathcal{C} + \mathcal{C} \begin{array}{c} \text{---} G^b \text{---} \\ \text{---} G^b \text{---} \end{array} \mathcal{C}, \quad \text{or} \quad \mathcal{T}_{ab,a'b'} = \sum_{klk'l'} \mathcal{C}_{ab,kl} G_{kk'}^b G_{ll'}^b \mathcal{C}_{a'b',k'l'}. \quad (\text{A12})$$

Thus, using the diagram technique, we found that the four-point resolvent $\hat{\mathcal{G}}$ is equal to

$$\mathcal{G}_{ab,a'b'} = \mathcal{L}_{ab,a'b'} + \mathcal{L}_{ab',a'b} - \mathcal{R}_{ab,a'b'}, \quad (\text{A13})$$

where the four-point matrix $\hat{\mathcal{L}}$ is defined as the solution of the equation

$$\hat{\mathcal{L}} = \hat{\mathcal{R}} + \hat{\mathcal{R}} : \hat{\mathcal{T}} : \hat{\mathcal{L}}, \quad (\text{A14})$$

known as the two-particle Dyson equation.

Appendix B: A model of uncorrelated bonds

In this Section, we provide a simple model, which represents all the properties of the strongly disordered medium discussed before. This model can be easily used to produce the corresponding force-constant matrices using random number generation.

Different bonds have different spatial positions and involve different sets of degrees of freedom. To describe the spatial correlations of non-affine deformations in the simplest form, it is further assumed that different bonds are uncorrelated with each other, leading to a covariance of the following form [20]:

$$\mathcal{C}_{ab,kl} = C_{ab}^{(k)} \delta_{kl}. \quad (\text{B1})$$

As a result, k -th column of the matrix \hat{A} has the Gaussian distribution with the covariance matrix $\hat{C}^{(k)}$, which obeys sum rules (57) and (58). The nonzero elements of $\hat{C}^{(k)}$ form a small group of nearest interacting atoms.

As it follows from the Dyson-Schwinger equations (26)–(27), the assumption (B1) leads to the diagonal form of \hat{G}^b :

$$G_{kl}^b = \varkappa_k \delta_{kl}. \quad (\text{B2})$$

For a uniform and isotropic (on average) system under consideration, $\varkappa_k = \varkappa$. Therefore, the solution of the Dyson-Schwinger equations (26)–(27) in the limit $\epsilon \rightarrow 0$ takes the form

$$\hat{G}^b = \varkappa \hat{1}, \quad \hat{G} = \frac{1}{\varkappa} \left(\sum_k \hat{C}^{(k)} \right)^{-1}. \quad (\text{B3})$$

Since $\hat{G}^{-1} = \varkappa \sum_k \hat{C}^{(k)}$, its Fourier transform is

$$(G^{-1})_{\alpha\beta}(\mathbf{q}) = \frac{\varkappa}{N} \sum_{ijk} C_{i\alpha j\beta}^{(k)} e^{i\mathbf{q} \cdot (\mathbf{r}_i^{\text{ref}} - \mathbf{r}_j^{\text{ref}})}. \quad (\text{B4})$$

For the isotropic distribution of bonds and $q \ll 1/a_0$, we obtain the usual form of Eq. (66) with Lamé moduli

$$\lambda = \varkappa \Lambda_{\alpha\beta\alpha\beta}, \quad (\text{B5})$$

$$\mu = \varkappa \Lambda_{\alpha\alpha\beta\beta}, \quad (\text{B6})$$

where the tensor

$$\Lambda_{\alpha\beta\gamma\eta} = \frac{1}{N} \sum_{ijk} C_{i\alpha j\beta}^{(k)} (r_{i\gamma}^{\text{ref}} - r_{k\gamma}) (r_{j\eta}^{\text{ref}} - r_{k\eta}) \quad (\text{B7})$$

represents the average properties of the bonds.

The four-point matrix $\hat{\mathcal{T}}$ has the form

$$\mathcal{T}_{ab,a'b'} = \varkappa^2 \sum_k C_{ab}^{(k)} C_{a'b'}^{(k)}. \quad (\text{B8})$$

One can note that matrices $\hat{C}^{(k)}$ are not the basis matrices of $\hat{\mathcal{T}}$ orthogonal with the weight $\hat{\mathcal{R}}$ since

$$P_{kl} = \sum_{aba'b'} G_{ab} C_{ba'}^{(k)} G_{a'b'} C_{b'a}^{(l)} \quad (\text{B9})$$

is not equal to $N'_{\text{dof}} \delta_{kl}$ and does not fulfill the orthogonality criterion (41). However, we can apply the Fourier transform

$$C_{ab}^{(\mathbf{p})} = \sum_k C_{ab}^{(k)} e^{i\mathbf{p} \cdot \mathbf{r}_k}, \quad (\text{B10})$$

where \mathbf{r}_k is the coordinate of the center of the bond k . Similarly,

$$P(\mathbf{p}) = \frac{1}{N_b} \sum_{kl} P_{kl} e^{i\mathbf{p} \cdot (\mathbf{r}_k - \mathbf{r}_l)}. \quad (\text{B11})$$

Thus, the matrix $\hat{\mathcal{T}}$ contains only one branch in the simple model under consideration:

$$\mathcal{T}_{ab,a'b'} = \sum_{\mathbf{p}} S_{ab}^{(\mathbf{p})} \theta(\mathbf{p}) S_{a'b'}^{(\mathbf{p})\dagger}, \quad (\text{B12})$$

where the eigenmatrices and eigenvalues are

$$S_{ab}^{(\mathbf{p})} = \sqrt{\frac{1 - \varkappa}{P(\mathbf{p})}} C_{ab}^{(\mathbf{p})}, \quad (\text{B13})$$

$$\theta(\mathbf{p}) = \varkappa^2 P(\mathbf{p}). \quad (\text{B14})$$

For small $p \ll 1/a_0$, we have the eigenfunction

$$\hat{S}^{(\mathbf{p})} = \hat{G}^{-1}(\mathbf{p}) + \mathcal{O}(p^2), \quad (\text{B15})$$

whereas the eigenvalue is

$$\theta(\mathbf{p}) = 1 - \varkappa - \xi_0^2 p^2 + \mathcal{O}(p^4), \quad (\text{B16})$$

where

$$\xi_0^2 = \frac{\varkappa^2}{2dN_b} \sum_{kl} P_{kl} (\mathbf{r}_k - \mathbf{r}_l)^2. \quad (\text{B17})$$

Thus, in this model of uncorrelated bonds, the approximation $\hat{S}^{(0)} \approx \hat{G}^{-1}$ is fulfilled and $\tilde{\lambda} = \lambda$, $\tilde{\mu} = \mu$, along with $\tilde{\varkappa} = \varkappa$ describe the spatial correlations of non-affine deformations as described by the equations in Section V. The length scale $\xi = \xi_0/\sqrt{\varkappa}$ coincides exactly with the one derived in [20].

Appendix C: Non-affine correlation functions

For the general strain tensor ε , the non-affine correlation function is $K_{\alpha\beta}(\mathbf{q}) = K_{\alpha\beta}^{\text{ld}}(\mathbf{q}) + K_{\alpha\beta}^{\text{tw}}(\mathbf{q})$ with

$$K_{\alpha\beta}^{\text{ld}}(\mathbf{q}) = \frac{(\tilde{\lambda} + \tilde{\mu})(\varepsilon_{\gamma\gamma})^2 + (\tilde{\lambda} + 3\tilde{\mu})\varepsilon_{\gamma\eta}\varepsilon_{\gamma\eta}}{4\tilde{\varkappa}} \left(\frac{\tilde{\mu}}{\mu^2} \frac{q^2 \delta_{\alpha\beta} - q_\alpha q_\beta}{q^4} + \frac{\tilde{\lambda} + 2\tilde{\mu}}{(\lambda + 2\mu)^2} \frac{q_\alpha q_\beta}{q^4} \right), \quad (\text{C1})$$

$$K_{\alpha\beta}^{\text{tw}}(\mathbf{q}) = \frac{v_\alpha(\mathbf{q})v_\beta(\mathbf{q})}{\tilde{\varkappa}(1 + \xi^2 q^2)}, \quad v_\alpha(\mathbf{q}) = \frac{(\tilde{\lambda} + \tilde{\mu})\varepsilon_{\beta\beta}q_\alpha}{2(\lambda + 2\mu)q^2} + \frac{\tilde{\lambda} + 3\tilde{\mu}}{2\mu q^2} \left(\varepsilon_{\alpha\beta}q_\beta - \frac{\lambda + \mu}{\lambda + 2\mu} \frac{q_\alpha \varepsilon_{\beta\gamma} q_\beta q_\gamma}{q^2} \right). \quad (\text{C2})$$

For volumetric deformation $\varepsilon_{\alpha\beta} = \varepsilon\delta_{\alpha\beta}$, it simplifies to

$$K_{\alpha\beta}^{\text{ld}}(\mathbf{q}) = c_0 \frac{q^2 \delta_{\alpha\beta} - q_\alpha q_\beta}{q^4} + c_1 \frac{q_\alpha q_\beta}{q^4}, \quad (\text{C3})$$

$$K_{\alpha\beta}^{\text{tw}}(\mathbf{q}) = c_2 \frac{q_\alpha q_\beta}{(1 + \xi^2 q^2) q^4}, \quad (\text{C4})$$

where

$$c_0 = \frac{d(d(\tilde{\lambda} + \tilde{\mu}) + \tilde{\lambda} + 3\tilde{\mu})\tilde{\mu}}{4\tilde{\kappa}\mu^2} \varepsilon^2, \quad c_1 = \frac{d(d(\tilde{\lambda} + \tilde{\mu}) + \tilde{\lambda} + 3\tilde{\mu})(\tilde{\lambda} + 2\tilde{\mu})}{4\tilde{\kappa}(\lambda + 2\mu)^2} \varepsilon^2, \quad c_2 = \frac{(d(\tilde{\lambda} + \tilde{\mu}) + \tilde{\lambda} + 3\tilde{\mu})^2}{4\tilde{\kappa}(\lambda + 2\mu)^2} \varepsilon^2. \quad (\text{C5})$$

The Fourier transform (81) gives the corresponding spatial correlation functions $K_{\alpha\beta}^{\text{ld}}(\mathbf{r})$ and $K_{\alpha\beta}^{\text{tw}}(\mathbf{r})$. In three dimensions ($d = 3$):

$$K_{\alpha\beta}^{\text{ld}}(\mathbf{r}) = \frac{(c_0 + c_1)\delta_{\alpha\beta}}{8\pi n_{\text{at}} r} + \frac{(c_0 - c_1)r_\alpha r_\beta}{8\pi n_{\text{at}} r^3}, \quad (\text{C6})$$

$$K_{\alpha\beta}^{\text{tw}}(\mathbf{r}) = \frac{c_2}{4\pi n_{\text{at}}} \left[\frac{(r^2 - 2\xi^2)\delta_{\alpha\beta}}{2r^3} + \frac{(6\xi^2 - r^2)r_\alpha r_\beta}{2r^5} + e^{-r/\xi} \left(\frac{\xi(r + \xi)\delta_{\alpha\beta}}{r^3} - \frac{(r^2 + 3r\xi + 3\xi^2)r_\alpha r_\beta}{r^5} \right) \right]. \quad (\text{C7})$$

In two dimensions ($d = 2$):

$$K_{\alpha\beta}^{\text{ld}}(\mathbf{r}) = -\frac{(c_0 + c_1)\delta_{\alpha\beta}}{4\pi n_{\text{at}}} \ln \frac{r}{r_0} + \frac{(c_0 - c_1)r_\alpha r_\beta}{4\pi n_{\text{at}} r^2}, \quad (\text{C8})$$

$$K_{\alpha\beta}^{\text{tw}}(\mathbf{r}) = -\frac{c_2}{4\pi n_{\text{at}}} \left[\delta_{\alpha\beta} \left(\frac{2\xi^2}{r^2} + \ln \frac{r}{r_0} - \frac{2\xi}{r} K_1(r/\xi) \right) + \frac{r_\alpha r_\beta}{r^2} \left(1 - \frac{4\xi^2}{r^2} + 2K_2(r/\xi) \right) \right], \quad (\text{C9})$$

where r_0 is the normalization length of the order of the system size (the integral diverges for an infinite system) and $K_\nu(x)$ is the modified Bessel function of the second kind, which has exponential asymptotic behavior $K_\nu(x) \simeq \sqrt{\pi/2x} e^{-x}$ for large x .

For the general strain tensor ε , the correlation function of the divergence of the non-affine displacement field defined by Eq. (87) can be written as

$$K_{\text{div}}(\mathbf{q}) = c_1 + \frac{c_2(\mathbf{q})}{1 + \xi^2 q^2}, \quad (\text{C10})$$

where

$$c_1 = \frac{\tilde{\lambda} + 2\tilde{\mu}}{4\tilde{\kappa}(\lambda + 2\mu)^2} \left((\tilde{\lambda} + \tilde{\mu})(\varepsilon_{\alpha\alpha})^2 + (\tilde{\lambda} + 3\tilde{\mu})\varepsilon_{\alpha\beta}\varepsilon_{\alpha\beta} \right), \quad (\text{C11})$$

$$c_2(\mathbf{q}) = \frac{1}{4\tilde{\kappa}(\lambda + 2\mu)^2} \left((\tilde{\lambda} + \tilde{\mu})(\varepsilon_{\alpha\alpha})^2 + (\tilde{\lambda} + 3\tilde{\mu}) \frac{\varepsilon_{\alpha\beta} q_\alpha q_\beta}{q^2} \right)^2. \quad (\text{C12})$$

For $\varepsilon_{\alpha\beta} = \varepsilon\delta_{\alpha\beta}$, c_1 and $c_2(\mathbf{q})$ reduce to c_1 and c_2 given by Eq. (C5), respectively.

The correlation function of the rotor of the non-affine displacement field defined by Eq. (97) can be written as

$$K_{\text{rot}}(\mathbf{q}) = c_3 + \frac{c_4(\mathbf{q})}{1 + \xi^2 q^2}, \quad (\text{C13})$$

where

$$c_3 = \frac{(d-1)\tilde{\mu}}{4\mu^2} \left((\tilde{\lambda} + \tilde{\mu})(\varepsilon_{\alpha\alpha})^2 + (\tilde{\lambda} + 3\tilde{\mu})\varepsilon_{\alpha\beta}\varepsilon_{\alpha\beta} \right), \quad (\text{C14})$$

$$c_4(\mathbf{q}) = \frac{(\tilde{\lambda} + 3\tilde{\mu})^2}{4\tilde{\kappa}\mu^2} \left(\frac{q_\alpha \varepsilon_{\alpha\beta} \varepsilon_{\beta\gamma} q_\gamma}{q^2} - \frac{(\varepsilon_{\alpha\beta} q_\alpha q_\beta)^2}{q^4} \right). \quad (\text{C15})$$

For the general strain tensor ε , the correlation functions $K_{\text{div}}(\mathbf{q})$ and $K_{\text{rot}}(\mathbf{q})$ are anisotropic. Their isotropic parts are:

$$K_{\text{div}}^{\text{iso}}(\mathbf{q}) = c_1 + \frac{c_2}{1 + \xi^2 q^2}, \quad (\text{C16})$$

$$K_{\text{rot}}^{\text{iso}}(\mathbf{q}) = c_3 + \frac{c_4}{1 + \xi^2 q^2}, \quad (\text{C17})$$

where c_1 and c_3 are defined in Eqs. (C14) and (C15), while the c_2 and c_4 are isotropic parts of $c_2(\mathbf{q})$ and $c_4(\mathbf{q})$, respectively:

$$c_2 = \frac{(d(\tilde{\lambda} + \tilde{\mu}) + \tilde{\lambda} + 3\tilde{\mu})^2 (\varepsilon_{\alpha\alpha})^2 + 2(\tilde{\lambda} + 3\tilde{\mu})^2 \frac{d\varepsilon_{\alpha\beta}\varepsilon_{\beta\alpha} - (\varepsilon_{\alpha\alpha})^2}{d+2}}{4\tilde{\kappa}(\lambda + 2\mu)^2 d^2}, \quad (\text{C18})$$

$$c_4 = \frac{(\tilde{\lambda} + 3\tilde{\mu})^2}{4\tilde{\kappa}\mu^2} \frac{d\varepsilon_{\alpha\beta}\varepsilon_{\beta\alpha} - (\varepsilon_{\alpha\alpha})^2}{d(d+2)}. \quad (\text{C19})$$

The Fourier transform (81) gives the corresponding spatial correlation functions $K_{\text{div}}^{\text{iso}}(\mathbf{r})$ and $K_{\text{rot}}^{\text{iso}}(\mathbf{r})$:

$$K_{\text{div}}^{\text{iso}}(\mathbf{r}) = \frac{c_1}{n_{\text{at}}} \delta(\mathbf{r}) + \frac{c_2}{n_{\text{at}}} D(\mathbf{r}), \quad (\text{C20})$$

$$K_{\text{rot}}^{\text{iso}}(\mathbf{r}) = \frac{c_3}{n_{\text{at}}} \delta(\mathbf{r}) + \frac{c_4}{n_{\text{at}}} D(\mathbf{r}). \quad (\text{C21})$$

The expressions of $K_{\text{div}}(\mathbf{q})$ and $K_{\text{rot}}(\mathbf{q})$ as well as $K_{\text{div}}(\mathbf{r})$ and $K_{\text{rot}}(\mathbf{r})$ for the particular case of the volumetric deformation are given in the main text in Section V.

-
- [1] P. W. Anderson, Through the glass lightly, *Science* **267**, 1615 (1995).
 - [2] K. Ngai, Why the glass transition problem remains unsolved?, *Journal of Non-Crystalline Solids* **353**, 709 (2007).
 - [3] G. B. McKenna and S. L. Simon, *50th Anniversary Perspective: Challenges in the dynamics and kinetics of glass-forming polymers*, *Macromolecules* **50**, 6333 (2017).
 - [4] W.-X. Zhou, Y. Cheng, K.-Q. Chen, G. Xie, T. Wang, and G. Zhang, Thermal conductivity of amorphous materials, *Advanced Functional Materials* **30**, 1903829 (2020).
 - [5] Y.-C. Hu and H. Tanaka, Origin of the boson peak in amorphous solids, *Nature Physics* **18**, 669 (2022).
 - [6] K. Yoshimoto, T. S. Jain, K. V. Workum, P. F. Nealey, and J. J. De Pablo, Mechanical heterogeneities in model polymer glasses at small length scales, *Physical Review Letters* **93**, 175501 (2004).
 - [7] M. Tsamados, A. Tanguy, C. Goldenberg, and J.-L. Barrat, Local elasticity map and plasticity in a model Lennard-Jones glass, *Physical Review E* **80**, 26112 (2009).
 - [8] H. Wagner, D. Bedorf, S. Küchemann, M. Schwabe, B. Zhang, W. Arnold, and K. Samwer, Local elastic properties of a metallic glass, *Nature Materials* **10**, 439 (2011).
 - [9] H. Mizuno, S. Mossa, and J.-L. Barrat, Measuring spatial distribution of the local elastic modulus in glasses, *Physical Review E* **87**, 42306 (2013).
 - [10] A. Zacccone, J. R. Blundell, and E. M. Terentjev, Network disorder and nonaffine deformations in marginal solids, *Physical Review B* **84**, 174119 (2011).
 - [11] S. Alexander, Amorphous solids: Their structure, lattice dynamics and elasticity, *Physics Reports* **296**, 65 (1998).
 - [12] A. Lemaître and C. Maloney, Sum rules for the quasi-static and visco-elastic response of disordered solids at zero temperature, *Journal of Statistical Physics* **123**, 415 (2006).
 - [13] R. Jana and L. Pastewka, Correlations of non-affine displacements in metallic glasses through the yield transition, *Journal of Physics: Materials* **2**, 045006 (2019).
 - [14] Q. Wen, A. Basu, P. A. Janmey, and A. G. Yodh, Non-affine deformations in polymer hydrogels, *Soft Matter* **8**, 8039 (2012).
 - [15] E. Del Gado, P. Ilg, M. Kröger, and H. C. Öttinger, Non-affine deformation of inherent structure as a static signature of cooperativity in supercooled liquids, *Physical Review Letters* **101**, 95501 (2008).
 - [16] C. Goldenberg, A. Tanguy, and J.-L. Barrat, Particle displacements in the elastic deformation of amorphous materials: Local fluctuations vs. non-affine field, *Europhysics Letters* **80**, 16003 (2007).
 - [17] F. Léonforte, A. Tanguy, J. P. Wittmer, and J.-L. Barrat, Inhomogeneous elastic response of silica glass, *Physical Review Letters* **97**, 055501 (2006).
 - [18] T. Damart, A. Tanguy, and D. Rodney, Theory of harmonic dissipation in disordered solids, *Physical Review B* **95**, 054203 (2017).
 - [19] Y. M. Beltukov, D. A. Conyuh, and I. A. Solov'yov, Local elastic properties of polystyrene nanocomposites increase significantly due to nonaffine deformations, *Physical Review E* **105**, L012501 (2022).
 - [20] D. A. Conyuh, A. A. Semenov, and Y. M. Beltukov, Effective elastic moduli of composites with a strongly disordered host material, *Physical Review E* **108**, 045004 (2023).

- [21] A. Tanguy, J. P. Wittmer, F. Leonforte, and J.-L. Barrat, Continuum limit of amorphous elastic bodies: A finite-size study of low-frequency harmonic vibrations, *Physical Review B* **66**, 174205 (2002).
- [22] F. Léonforte, R. Boissière, A. Tanguy, J. P. Wittmer, and J.-L. Barrat, Continuum limit of amorphous elastic bodies (III): Three dimensional systems, *Physical Review B* **72**, 224206 (2005), arXiv:cond-mat/0505610.
- [23] B. A. DiDonna and T. C. Lubensky, Nonaffine correlations in random elastic media, *Physical Review E* **72**, 066619 (2005).
- [24] C. E. Maloney, Correlations in the elastic response of dense random packings, *Physical Review Letters* **97**, 035503 (2006).
- [25] C. E. Maloney and M. O. Robbins, Anisotropic power law strain correlations in sheared amorphous 2D solids, *Physical Review Letters* **102**, 225502 (2009).
- [26] F. Varnik, S. Mandal, V. Chikkadi, D. Denisov, P. Olsson, D. Vågberg, D. Raabe, and P. Schall, Correlations of plasticity in sheared glasses, *Physical Review E* **89**, 040301 (2014).
- [27] L. Meenakshi and B. S. Gupta, Characteristics and correlations of nonaffine particle displacements in the plastic deformation of athermal amorphous materials, *Soft Matter* **18**, 8626 (2022).
- [28] F. H. Stillinger, Supercooled liquids, glass transitions, and the Kauzmann paradox, *The Journal of Chemical Physics* **88**, 7818 (1988).
- [29] E. Lerner and E. Bouchbinder, Frustration-induced internal stresses are responsible for quasilocalized modes in structural glasses, *Physical Review E* **97**, 032140 (2018), arXiv:1711.11263 [cond-mat].
- [30] Y. M. Beltukov, V. I. Kozub, and D. A. Parshin, Ioffe-Regel criterion and diffusion of vibrations in random lattices, *Physical Review B* **87**, 134203 (2013).
- [31] D. A. Conyuh and Y. M. Beltukov, Random matrix approach to the boson peak and Ioffe-Regel criterion in amorphous solids, *Physical Review B* **103**, 104204 (2021).
- [32] T. S. Grigera, V. Martín-Mayor, G. Parisi, and P. Verrocchio, Vibrations in glasses and Euclidean random matrix theory, *Journal of Physics: Condensed Matter* **14**, 2167 (2002).
- [33] M. L. Manning and A. J. Liu, A random matrix definition of the boson peak, *EPL (Europhysics Letters)* **109**, 36002 (2015).
- [34] M. Baggioli, R. Milkus, and A. Zaccane, Vibrational density of states and specific heat in glasses from random matrix theory, *Physical Review E* **100**, 062131 (2019).
- [35] Y. M. Beltukov, Random matrix theory approach to vibrations near the jamming transition, *JETP Letters* **101**, 345 (2015).
- [36] A. Altieri, *Jamming and Glass Transitions: In Mean-Field Theories and Beyond*, Springer Theses (Springer International Publishing, Cham, 2019).
- [37] O. Narayan and H. Mathur, Vibrational spectrum of Granular packings with random matrices, *The European Physical Journal E* **47**, 19 (2024).
- [38] D. A. Conyuh and Y. M. Beltukov, Ioffe-Regel criterion and viscoelastic properties of amorphous solids, *Physical Review E* **103**, 042608 (2021).
- [39] Y. M. Beltukov and D. A. Parshin, Boson peak in various random-matrix models, *JETP Letters* **104**, 552 (2016).
- [40] G. Eichmann, A. Gómez, J. Horak, J. M. Pawłowski, J. Wessely, and N. Wink, Bound states from the spectral Bethe-Salpeter equation, *Physical Review D* **109**, 096024 (2024).
- [41] J. W. Helton, R. R. Far, and R. Speicher, Operator-valued semicircular elements: Solving a quadratic matrix equation with positivity constraints, *International Mathematics Research Notices* **2007**, 10.1093/imrn/rnm086 (2007).
- [42] O. H. Ajanki, L. Erdős, and T. Krüger, Stability of the matrix Dyson equation and random matrices with correlations, *Probability Theory and Related Fields* **173**, 293 (2019).
- [43] A. A. Maradudin, E. W. Montroll, G. H. Weiss, and L. P. Ipatova, *Theory of Lattice Dynamics in the Harmonic Approximation* (Academic Press, New York and London, 1971).
- [44] T. Mura, *Micromechanics of Defects in Solids*, edited by S. Nemat-Nasser and G. Æ. Oravas, *Mechanics of Elastic and Inelastic Solids*, Vol. 3 (Springer Netherlands, Dordrecht, 1987).
- [45] N. W. Ashcroft and N. D. Mermin, *Solid State Physics* (Harcourt College Publishers, New York, 1976).
- [46] L. Yan, E. DeGiuli, and M. Wyart, On variational arguments for vibrational modes near jamming, *EPL (Europhysics Letters)* **114**, 26003 (2016).
- [47] M. Shimada, H. Mizuno, M. Wyart, and A. Ikeda, Spatial structure of quasilocalized vibrations in nearly jammed amorphous solids, *Physical Review E* **98**, 060901 (2018).
- [48] A. P. Thompson, H. M. Aktulga, R. Berger, D. S. Bolintineanu, W. M. Brown, P. S. Crozier, P. J. In 't Veld, A. Kohlmeyer, S. G. Moore, T. D. Nguyen, R. Shan, M. J. Stevens, J. Tranchida, C. Trott, and S. J. Plimpton, LAMMPS - a flexible simulation tool for particle-based materials modeling at the atomic, meso, and continuum scales, *Computer Physics Communications* **271**, 108171 (2022).
- [49] G. Rossi, L. Monticelli, S. R. Puisto, I. Vattulainen, and T. Ala-Nissila, Coarse-graining polymers with the MARTINI force-field: Polystyrene as a benchmark case, *Soft Matter* **7**, 698 (2011).
- [50] J. Guénolé, W. G. Nöhring, A. Vaid, F. Houllé, Z. Xie, A. Prakash, and E. Bitzek, Assessment and optimization of the fast inertial relaxation engine (FIRE) for energy minimization in atomistic simulations and its implementation in LAMMPS, *Computational Materials Science* **175**, 109584 (2020).
- [51] L. Gartner and E. Lerner, Nonlinear plastic modes in disordered solids, *Physical Review E* **93**, 011001 (2016).
- [52] G. Kapteijns, D. Richard, and E. Lerner, Nonlinear quasilocalized excitations in glasses. I. True representatives of soft spots, *Physical Review E* **101**, 032130 (2020), arXiv:1912.10930 [cond-mat].
- [53] C. Rainone, E. Bouchbinder, and E. Lerner, Pinching a glass reveals key properties of its soft spots, *Proceedings of the National Academy of Sciences* **117**, 5228 (2020).
- [54] Y. M. Beltukov and D. A. Parshin, Theory of sparse random matrices and vibrational spectra of amorphous solids, *Physics of the Solid State* **53**, 151 (2011).
- [55] A. A. Semenov, D. A. Konyuh, and Ya. M. Beltyukov, Nonaffine deformations and local elastic properties of amorphous nanostructures, *Physics of the Solid State* **64**, 1052 (2022).
- [56] S. Mandal, V. Chikkadi, B. Nienhuis, D. Raabe, P. Schall, and F. Varnik, Single-particle fluctuations and directional correlations in driven hard-sphere glasses, *Physical*

- Review E **88**, 022129 (2013).
- [57] C. S. O'Hern, L. E. Silbert, A. J. Liu, and S. R. Nagel, Jamming at zero temperature and zero applied stress: The epitome of disorder, *Physical Review E* **68**, 011306 (2003).
 - [58] Z. Zhang, N. Xu, D. T. N. Chen, P. Yunker, A. M. Alsayed, K. B. Aptowicz, P. Habdas, A. J. Liu, S. R. Nagel, and A. G. Yodh, Thermal vestige of the zero-temperature jamming transition, *Nature* **459**, 230 (2009).
 - [59] Z. Burda, A. Görlich, A. Jarosz, and J. Jurkiewicz, Signal and noise in correlation matrix, *Physica A: Statistical Mechanics and its Applications* **343**, 295 (2004).